

98-1-4-14

# **Assessing Values of Air Quality and Visibility at Risk From Wildland Fires**

Sue A. Ferguson, Steven J. McKay, David E. Nagel, Trent  
Piepho, Miriam L. Rorig, Casey Anderson, Lara Kellogg

Final Report for the Joint Fire Science Program

United States Department of Agriculture  
Forest Service  
Pacific Northwest Research Station  
November 2001

## EXECUTIVE SUMMARY

To assess values of air quality and visibility at risk from wildland fire in the United States, we generated a 40-year database that includes twice-daily values of wind, mixing height, and a ventilation index that is the product of wind and mixing height. The database provides the first available, nationally consistent map of surface wind and ventilation index. In addition, it is the longest climate record of mixing height in the country. We built the database into an interactive Ventilation Climate Information System (VCIS) that allows users to assess risk based on frequency patterns of poor, marginal, fair, and good ventilation conditions.

Attributes of the Ventilation Climate Information System:

- VCIS is accessed through an Internet map server at [www.fs.fed.us/pnw/fera/vent](http://www.fs.fed.us/pnw/fera/vent).
- The data were generated for 40 years at 1200 UTC (morning) and 0000 UTC (afternoon).
- The data cover the entire United States at 2.5' latitude-longitude (about 5 km) spatial resolution in the 48 contiguous states and Hawaii and at 5 km resolution in Alaska.
- Surface winds (10 meters above ground level) are generated with a single-level, hydrostatic mesoscale meteorology model.
- Mixing heights are generated by spatially interpolating radiosonde observations then the heights are adjusted to account for intersecting high terrain and local nighttime inversions.
- The ventilation index is a product of surface wind and mixing height. Because it uses surface winds instead of higher level trajectory winds, it is a conservative estimate of ventilation potential and most applicable to smoke that remains relatively close to the ground.
- Accuracy of the data has been checked thoroughly and is available on the web site to help users to determine any level of uncertainty.

Risk to values of air quality and visibility from wildland fire:

- The greatest risk occurs in the southeastern United States where the frequency of poor and marginal ventilation conditions is greatest and the number and density of sensitive receptors is greatest.
- The northern plains and deep valleys in the western United States also show high risk potential especially during the winter and at times during spring and autumn.
- High desert regions show the best potential for good ventilation conditions resulting in the least risk to values of air quality and visibility in these regions.
- In all places and at all times of the year, good ventilation conditions and low risk to values of air quality and visibility can occur.
- The likelihood of finding an opportunity for good ventilation on any given day or time for any point the landscape can be determined from frequency plots on the VCIS web server.
- The year-to-year variability of ventilation index and associated risk in any month and at any point on the landscape can be determined from frequency plots on the VCIS web server.

## 1.0 INTRODUCTION

With the increasing use of prescribed fire as a way of managing wildland areas in the United States, predicting the potential impacts and assessing risks are becoming more important. Of great concern is the effect of smoke on air quality and visibility. Although few prescribed fires emit enough to violate clean air standards (United States Environmental Protection Agency 1997), many people are sensitive to slight amounts of smoke, especially if they already experience respiratory problems like emphysema or asthma (Schwartz and others 1993; Lipsett and others 1997). Citizen complaints can cause active burning programs to be delayed, redesigned, or even terminated. Also, smoke can severely degrade visibility when combined with other pollutants or moisture. Not only can this detract from scenic vistas, but the degraded visibility from smoke has been known to cause severe traffic accidents (Achte-meier and others 1998).

Unfortunately, consistent and timely emission inventories from wildland biomass burning are difficult to obtain and summarize for a national risk assessment. Also, data on the timing and release rate of emissions, which determine whether smoke will be lofted into the atmosphere or stay close to the ground, are not routinely kept. Lacking detailed and accurate emissions data, it is assumed that a simple index of ventilation potential is sufficient to help determine useful aspects of the risks to air quality and visibility from biomass burning. Because ventilation potential is the product of wind and mixing height, its determination is straightforward. Also, current and forecast values of the ventilation index are well known by air quality regulators and are used for managing biomass smoke in many parts of the country (South Carolina Forestry Commission, 1996; Wade 1989; USDA-Forest Service, Southern Forest Experiment Station 1976; Utah Administrative Code 2001).

By developing ventilation potential as a spatial database it can be overlain with other elements of risk for a more complete assessment of the impact of prescribed fire in wildland areas of the United States. Certain aspects of ventilation climatology already are well known by air pollution managers. For instance, low mixing heights and poor ventilation are common in coastal areas of the United States where moist marine air increases static stability (Holzworth 1972, Holzworth and Fisher 1979). Poor ventilation also is common everywhere at night when radiative cooling at the surface increases atmospheric stability. What is not known, however, is the probability of poor ventilation on any given day at any selected spot on the landscape. A long time series of high-resolution spatial data can help determine such probabilities.

Because we were tasked to generate a reasonable assessment of risk within two years, it was important to develop an accurate database in a short amount of time. We decided that spatial detail was important because most climate summaries are too coarse for application to land management. Also, a long time series was critical to capture naturally varying patterns in climate and to compensate for missing values, and it was important to simulate the diurnal changes. To this end, we generated a 40-year time series at 0000 Universal Time Coordinated (UTC) and 1200 UTC each day.<sup>1</sup> The

---

<sup>1</sup> The times, 0000 UTC and 1200 UTC, correspond to standard time in Greenwich, England, or Greenwich Mean time (GMT), and are called synoptic times because measurements collected all over the world occur simultaneously at these times to provide a consistent synopsis of the weather. It is morning in most of the U.S. at 1200 UTC and afternoon of the preceding day at 0000 UTC. For example, 1200 UTC on December 1st is 4am (04:00) December 1st in San Francisco, whereas 0000 UTC on December 1st is 4pm (16:00) November 30th in San Francisco. The letter Z, which is short for Zulu, is used as a nickname for UTC (e.g., 0Z and 12Z).

generated values of wind, mixing height, and ventilation index cover the United States at a horizontal grid spacing of 2.5 minute latitude/longitude (about 5 km), except Alaska where the grid spacing is fixed at 5 km  $\times$  5 km map projections (see Appendix 1).

Because we needed to generate the high-resolution climate information in a relatively short amount of time, relatively simple tools were used to derive data values and several simplifying assumptions were made. We tried to maintain physical reasonableness, however, and checked our results frequently against observations and common knowledge. Anytime data are derived, however, whether by spatially interpolating observations or physical models, accuracy and reliability are influenced. Therefore, details on the derivation process, assumptions, and methods of smoothing and parameterization are given to help users evaluate uncertainty in subsequent risk assessments. The first few sections of this report explain in detail the technical development of each meteorological component. Section 2 discusses the development of the surface wind fields, Section 3 covers the mixing height derivation, and Section 4 explains calculation of the ventilation index. We have highlighted key elements that may be of value to land managers at the end of each section.

After developing the spatial database, we assessed values of air quality and visibility at risk from wildland fire by grouping the ventilation index into large areas representing regional airsheds. The variation in space and time between each airshed and among individual airsheds is discussed in Section 5, with supporting data shown in Appendix 3.

With over 100 GigaBytes of data we cannot summarize everything effectively in a manuscript. Therefore, we made all the data and documentation available through a web site that includes an interactive map server <[www.fs.fed.us/pnw/fera/vent](http://www.fs.fed.us/pnw/fera/vent)>. The interactive Ventilation Climate Information System (VCIS) allows users to map monthly values of ventilation index with sensitive receptors, natural and political boundaries, and topography. In addition, users can zoom or print maps and it may be possible to import web-generated maps into their own GIS application. At any time, a summary of daily, monthly, and annual statistics for each variable at any point can be obtained by simple mouse click. Appendix 2 explains how to interpret the VCIS map products and graphs and a guide to the VCIS web site is given in Appendix 4.

## 2.0 WIND

To generate surface winds, we modified the single-level hydrostatic flow model of Danard (1977), Dempsey (1985), and Mass and Dempsey (1985). Various versions of the model have been successfully used to simulate sea-land breezes in Israel (Alpert 1988; Alpert and Getino 1988; Alpert et al. 1988), orographic flow fields for alpine precipitation forecasting (Speers and Mass 1986), and wind climates in the northwestern United States (Ruthford and Ferguson 2002). We modified the model to accommodate a spatially varying lapse rate<sup>2</sup> and run on a message-passing parallel computing platform. In addition, we modified the finite difference calculations to make them more stable and increase success rate in converging to a physically reasonable solution. We call our modified version of the Danard, Mass, and Dempsey model, WINFLO. We chose to use WINFLO to

---

<sup>2</sup> The spatially varying lapse rate was based on work supported by Dr. Sue Ferguson and performed by Ms. Shokoofeh Nowbakht under the direction of Professor David Dempsey, San Francisco State University.

generate surface winds over the large domain of the United States and the long, 40-year time period because of its rapid computation, reasonably accurate output, and success in a variety of applications.

Even though we had a high-speed, parallel computing platform of 40 850 MHz processors to run the model twice daily for 40 years, we needed to turn off the heating and cooling component within WINFLO to speed computations. This allowed us to complete the simulations within months instead of years. The heating and cooling component is designed to capture heat fluxes between the ground surface and atmosphere. Without the component, resulting winds are considered applicable to diurnally neutral times near sunrise and sunset. This means that the model will not resolve sea breezes or slope flows if they are not reflected in the 85 kPa heights and temperatures at 1200 UTC or 0000 UTC.

WINFLO uses sigma coordinates (terrain-following surfaces of constant pressure), with the single-layer sigma surface representing about 10 m above ground level. Only 2 classes of land surface are used, forested land and open water, having drag coefficients of 0.015 and 0.0014, respectively. While we did not find significant differences in model results when we changed the drag coefficient over land during tests in Oregon, we expect that the gross land-use categories may cause the model to underestimate surface winds over broad flat areas and grass lands.

As a hydrostatic model, WINFLO functions best when vertical motions are small compared to horizontal motions. Hydrostatic assumptions typically are inappropriate for horizontal scales less than about 5 km and during strongly dynamic events such as thunderstorms and gusting fronts. To accommodate the hydrostatic assumption, we kept the horizontal grid resolution near 5 km and created upper ( $8^{\circ}\text{C}/\text{km}$ ) and lower ( $3.5^{\circ}\text{C}/\text{km}$ ) bounds for the lapse rate. Lapse rates were calculated between the 85 kiloPascals (kPa)<sup>3</sup> and 50 kPa vertical levels. Observed values rarely exceeded  $8^{\circ}\text{C}/\text{km}$  but occasionally were less than  $3.5^{\circ}\text{C}/\text{km}$ . This forces some smoothing that would cause gusty surface winds to be underestimated by the model. This condition does not affect strong, sustained storm winds that are successfully simulated by WINFLO.

The upper-boundary initialization data were from the NCEP Reanalysis package (Kalnay et al. 1996). We chose to initialize the model with data from the 85 kPa level. This height usually is measured at about 1500 meters above sea level (asl), which is below the height of many mountain ranges in the western United States. However, at the resolution of the Reanalysis data, the western mountains are represented as highly smoothed undulations and the 85 kPa height seems to appropriately represent conditions above major orographic influences while reasonably reflecting surface conditions. For example, we simulated winds over the Sawtooth Mountains in Idaho, which consistently rise above 2500 meters asl, with both an 85 kPa reference height and a 70 kPa reference height (about 3000 m asl). When comparing model output with observations, including many high-elevation wind measurements from the interagency RAWs network (United States Department of Interior 1995), we found little difference in model performance between the two tests except that the model performed slightly better at turning winds through the terrain patterns when using data from the 85 kPa reference level than when using data from the 70 kPa level. Also, results from the 85 kPa height were consistently better at lower elevation sites.

---

<sup>3</sup> One kPa = 10 millibars (mb). Therefore, 85 kPa = 850 mb.

## 2.1 Observed vs. Modeled Wind

Surface winds are strongly influenced by small-scale undulations in terrain and land cover. Therefore, wind observations that are measured by anemometers are influenced by and represent conditions below the resolution of the model terrain and land-use grids and may not represent the larger-scale wind field. In addition, anemometers usually have stall speeds that prevent accurate recording when winds speeds are below about 1 m/s, they can be placed poorly in relation to buildings, towers, and other instruments, and often are poorly maintained. Therefore, it can be difficult to compare model-derived winds with observations. In each region, however, we asked local climatologists to review the wind maps to determine if patterns appeared reasonable.

The observations we selected for comparison came from NOAA National Weather Service (NWS) primary observing stations (National Renewable Laboratory 1992; National Climatic Data Center 1997). Data from local and regional networks, such as the interagency RAWs network (United States Department of Interior 1995), did not have adequate quality or consistency for model verification over the entire country and in all seasons.

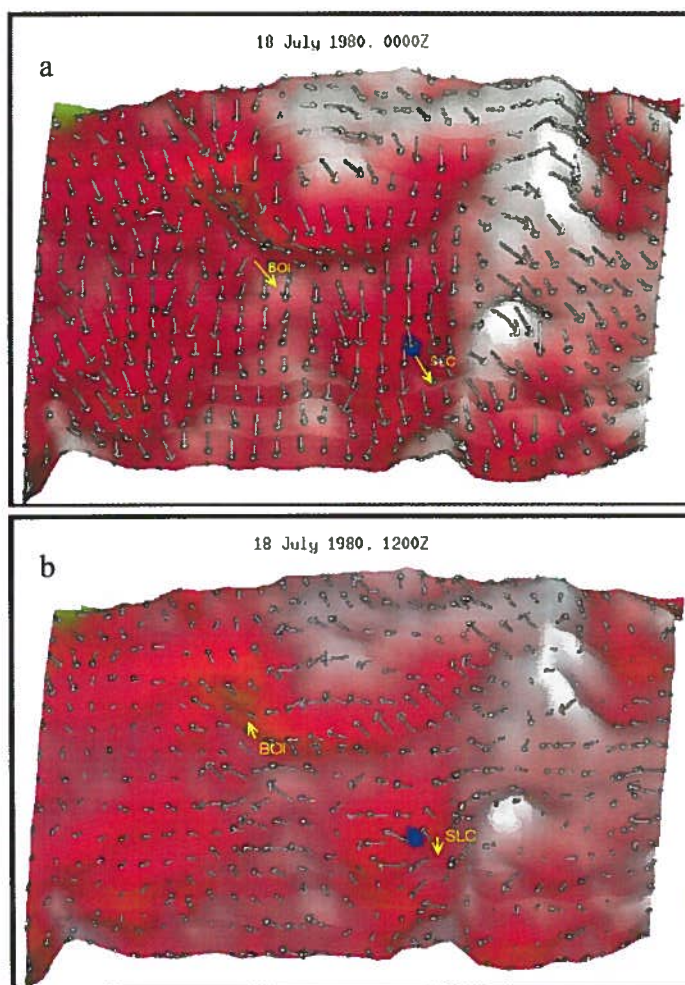


**Figure 2.1.** Modeled surface wind patterns over northern Utah and southern Idaho on 18 July 1980 for a) 0000 UTC and b) 1200 UTC. Observed winds at Salt Lake City, Utah (SLC) and Boise, Idaho (BOI) are shown in yellow.

To compare modeled winds with observed winds, we qualitatively analyzed general flow patterns, developed grouped statistics, and compared observed to modeled winds at each observation location. Figure 2.1 is an example of one of our qualitative plots that illustrates how general flow patterns compare with observations at specific times in a small region centered over southern Idaho and northern Utah. During the afternoon (Figure 2.1a), observed winds at Boise, Idaho (BOI) and Salt Lake City, Utah (SLC) were from the northwest at about 10 m/s. Modeled winds in the Boise area were generally from the northwest at about 8 m/s but turning north-northeasterly away from the central valley. Modeled winds over Salt Lake City were generally north-northwesterly at about 8 m/s. During the morning (Figure 2.1b), both modeled and observed winds at Boise became slower and turned southeasterly. While observed winds over Salt Lake City appeared from due north in the morning, modeled winds around the area were variable from southeast to northeast. Away from the observation points, flow patterns appear consistent with typical diurnal wind patterns (upvalley during the late afternoon and downvalley in the

early morning) and expected channel flow through gaps and valleys. Therefore, while minor inconsistencies occur at the observation points, the general flow pattern is physically consistent and realistic. Other similar subjective comparisons resulted in the same conclusions.

In addition to subjective comparisons, we calculated error statistics for each season. While statistical errors may seem high, it does not mean that the models are grossly inaccurate. Anemometers respond to very subtle features of land cover and terrain that are below the resolution of model grid spacing. Also, there may be differences in timing or errors in the observations themselves that can cause large differences. Therefore, statistical error summaries are more useful in highlighting inherent biases and tracking spatial or temporal inconsistencies rather than an exact evaluation of accuracy. We calculated differences in wind speed, wind direction, and vector wind. Vector winds are simply the east-west and north-south components of a wind vector whose length is represented by speed. Vector wind differences ( $vwd$ ) account for differences in speed and direction simultaneously and are calculated as:

$$vwd = \sqrt{(Um - Uo)^2 + (Vm - Vo)^2}, \text{ where } U = Ws \times \sin(Wd), \text{ and } V = Ws \times \cos(Wd),$$

with  $Ws$  = wind speed,  $Wd$  = wind direction,  $\pi$  = pi, and subscripts  $m$  = modeled and  $v$  = observed.

A number of different statistics were calculated for each season: winter (December, January, February), spring (March, April, May), summer (June, July, August), and autumn (September, October, November) as follows.

- 1) **Mean error** is the average of model minus observed. It shows if there are consistent biases but allows positive and negative biases to cancel each other out.
- 2) **Mean absolute error** is the average of the absolute value of model minus observed. It demonstrates the magnitude of difference.
- 3) **Root Mean Square (RMS) Error** is the square root of the difference between the square of the model and the square of the observed. This causes large differences to be weighted more than small differences. The lower the RMS error, the fewer large differences. If the model and observed values are identical, the RMS error would be zero.

Examples of some statistical results are shown in Table 2.1. Ten years of modeled surface wind in the northwestern United States from WINFLO at 2.5' latitude-longitude (about 5km) spatial resolution is compared with about 2 years of modeled surface winds from the Northwest Real-time MM5 meteorological model (Ferguson 2001) for a subset of the same domain at 4 km spatial resolution. The MM5 surface winds were derived from its lowest sigma level in 1998, which was about 40 meters above ground level (agl) then adjusted to 10 meters agl.<sup>4</sup> For this comparison, winds were represented in knots (knots x 0.515 = m/s).

Negative mean errors in wind speed for WINFLO indicate that modeled winds may be frequently slower than observed winds. Positive mean errors in MM5 suggest that modeled winds may be frequently higher than observed winds. Slowest biases in both models occur during spring and summer. This may be due to the inability of models to capture gusty winds associated with strong convection. Slow biases in WINFLO average less than 1 knot (0.5 m/s) at most times in most

---

<sup>4</sup> For a description of the Northwest Real-time model and verification methods see <<http://www.atmos.washington.edu/mm5rt/>>

Table 2.1. Error statistics between modeled and observed winds in the Northwest region. (a) WINFLO with 28 observations in 10 years. (b) MM5 with over 1000 observations in about 2 years. For this comparison, winds were represented in knots (knots x 0.515 = m/s).

Winflo		a		All				Observed Wind Speed >5 Knots			
Metric	Hour	Season	Mean Error	Mean Abs Error	Root MSE	Count	Mean Error	Mean Abs Error	Root MSE	Count	
Direction (degrees)	0Z	Winter	4.361	63.692	82.301	21005	1.681	52.425	71.320	14645	
		Spring	0.466	55.884	73.037	24684	0.573	52.490	69.297	21994	
		Summer	-10.184	58.935	76.089	15404	-10.378	56.357	73.460	13902	
		Autumn	0.291	59.934	77.798	12341	0.370	53.132	70.962	9783	
	12Z	Winter	5.037	69.840	88.102	20406	-1.597	53.383	73.009	11899	
		Spring	-1.339	70.547	87.818	23914	-1.930	59.827	79.007	14243	
		Summer	-5.131	77.521	94.091	14875	-3.517	69.711	89.182	8296	
		Autumn	3.395	71.713	89.002	11894	1.715	57.278	76.852	6673	
Speed (knots)	0Z	Winter	-0.697	3.879	5.185	21005	-2.275	4.027	5.458	14645	
		Spring	-3.878	4.940	6.368	24684	-4.596	5.213	6.635	21994	
		Summer	-3.482	4.807	6.131	15404	-4.170	4.962	6.303	13902	
		Autumn	-2.023	3.966	5.124	12341	-3.180	4.209	5.379	9783	
	12Z	Winter	0.976	4.010	5.257	20406	-1.148	3.772	5.171	11899	
		Spring	-0.093	3.437	4.389	23914	-2.064	3.441	4.402	14243	
		Summer	-0.222	3.245	4.105	14875	-2.389	3.273	4.091	8296	
		Autumn	0.611	3.635	4.621	11894	-1.505	3.479	4.476	6673	
Vector Wind Differences (knots)	0Z	Winter	6.931	6.931	8.175	21005	7.586	7.586	8.880	14645	
		Spring	8.197	8.197	9.371	34684	8.562	8.562	9.711	21994	
		Summer	8.359	8.359	9.424	15404	8.600	8.600	9.671	13902	
		Autumn	7.171	7.172	8.263	12341	7.659	7.659	8.748	9783	
	12Z	Winter	6.849	6.849	8.013	20406	7.424	7.424	8.726	11899	
		Spring	6.167	6.169	7.077	23914	6.809	6.809	7.732	14243	
		Summer	5.968	5.968	6.814	14875	6.770	6.770	7.593	8296	
		Autumn	6.279	6.279	7.241	11894	6.933	6.933	7.939	6673	

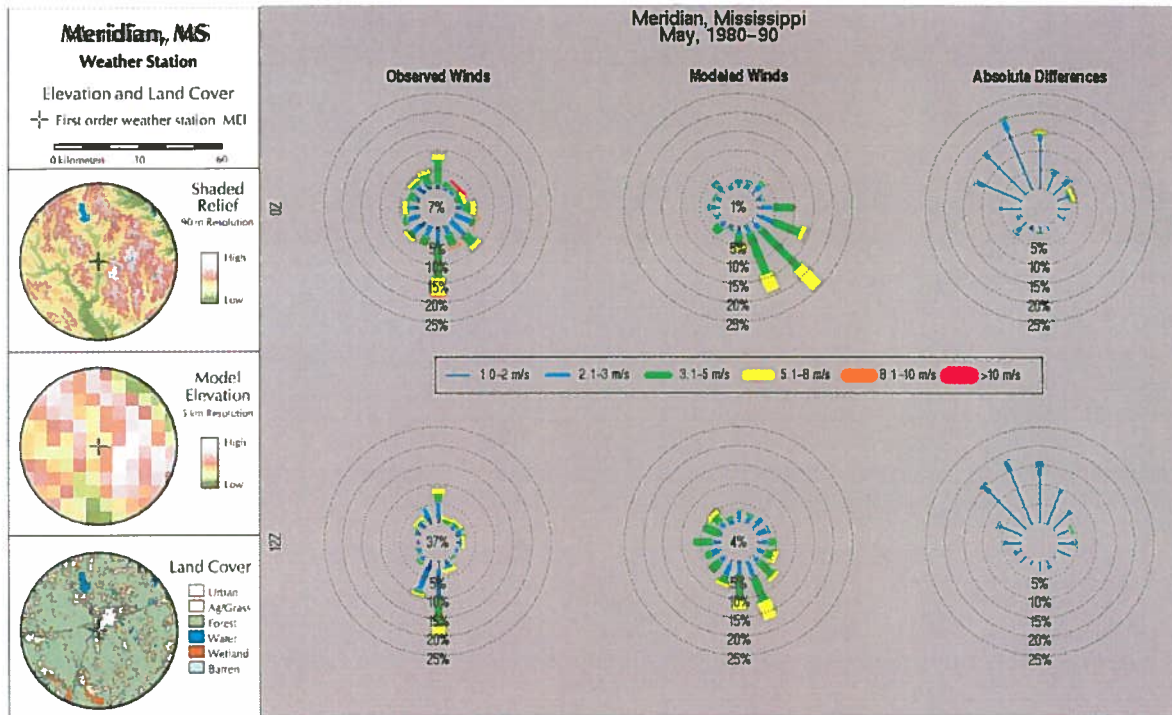
  

MM5		b		All				>5 Knots			
Metric	Hour	Season	Mean Error	Mean Abs Error	Root MSE	Count	Mean Error	Mean Abs Error	Root MSE	Count	
Direction	0Z	Winter	26.978	59.887	77.619	2981	25.72	46.892	63.013	1926	
		Spring	4.777	58.341	76.342	6953	11.081	43.98	62.705	3011	
		Summer	0.248	63.22	80.764	7707	12.311	46.729	65.347	2553	
		Autumn	10.895	66.078	83.827	6855	15.078	44.357	60.592	2403	
	12Z	Winter	20.188	60.575	79.072	3665	19.422	45.566	62.642	2302	
		Spring	7.17	54.434	72.172	9235	9.631	46.528	63.825	6116	
		Summer	10.993	47.877	64.711	8955	13.251	40.893	56.423	5723	
		Autumn	9.262	57.988	76.518	7858	11.832	42.985	60.05	3852	
Speed	0Z	Winter	2.931	5.359	6.974	3050					
		Spring	1.26	3.622	4.685	7081					
		Summer	1.92	3.654	4.633	7790					
		Autumn	2.568	4.318	5.531	6946					
	12Z	Winter	2.125	4.808	6.429	3748					
		Spring	-0.884	3.379	4.453	9523					
		Summer	-0.607	3.078	4.127	9230					
		Autumn	0.586	3.37	4.596	8004					
Vector Wind Differences	0Z	Winter	9.122	9.122	10.814	3050					
		Spring	5.623	5.623	6.841	7081					
		Summer	5.523	5.523	6.054	7796					
		Autumn	6.324	6.324	7.595	6946					
	12Z	Winter	8.084	8.084	9.746	3748					
		Spring	6.014	6.014	7.138	9523					
		Summer	5.363	5.363	6.396	9230					
		Autumn	5.574	5.574	6.978	8004					

seasons. During the afternoon, however, biases average about -4 knots (2 m/s) in spring and summer, and about -2 knots (1 m/s) in autumn.

Mean absolute errors in direction for WINFLO ranged from about 56° in spring afternoons to 78° in summer mornings while MM5 errors ranged from about 48° to 66°. Mean absolute errors in WINFLO's speed ranged from 3.2 knots (1.6 m/s) in summer mornings to 4.9 knots (2.5 m/s) in spring afternoons while MM5 errors ranged from 3.0 knots (1.5 m/s) to 5.4 knots (2.8 m/s). RMS errors in direction range from about 73° to 89° for WINFLO and about 65° to 84° for MM5, suggesting that large differences between modeled and observed direction is possible. RMS errors in speed range from 4.1 knots (2.1 m/s) to 6.4 knots (3.3 m/s) in WINFLO and from 5.1 knots (2.6 m/s) to 7.0 knots (3.6 m/s) in MM5. Vector wind differences in WINFLO (6.8 knots to 9.4 knots) were in the same range as in MM5 (6.0 knots to 10.8 knots).

Our most extensive error analysis was accomplished by plotting the frequency of modeled and observed wind speed and direction at each observation location (Figure 2.2). Also included are maps surrounding each observation station of the model terrain at 2.5' latitude-longitude or 5km resolution and fine-resolution terrain and land use, both at 90-meter resolution. This allows the user to distinguish whether differences between modeled and observed winds at that location are due to smoothing of terrain and land-use in the model or caused by parameterized model physics.



**Figure 2.2.** Model vs. observed winds at Meridian, Mississippi. Shaded relief, model elevation, and land cover are shown in circles on the left. Wind roses of observed and modeled winds and polar plots of absolute differences are shown on the right for both 0000 UTC (top row) and 1200 UTC (bottom row).

Plots were generated for each month and each synoptic time period, allowing for examination of seasonal and diurnal performance. Directional difference is determined by subtracting each observation from its corresponding modeled value. When observed winds are less than 1 m/s, however, they and the corresponding modeled winds are excluded from difference calculations to account for the threshold wind speed of most anemometers. Differences between modeled and observed wind speeds are presented as positive values, not distinguishing between overestimation and underestimation, hence the term “absolute difference.” Difference in speed is represented by line thickness, using the same speed classes as wind roses, except that differences less than 1 m/s are not a separate category, causing the thinnest line segments to represent all wind speed differences less 2 m/s. Difference in direction is represented by the angle in which a ray radiates out from the center of the plot. Straight up indicates essentially no difference (within 11.25 degrees). An angle of 90 degrees indicates that the modeled winds differ from the observed winds by 90 degrees in the clockwise direction (i.e., an observed direction of northeast and a modeled direction of southeast).

Comparing the polar plots of differences to terrain and land use around the observation station help determine whether the model is failing because of its simplified physics and numerical schemes or because its terrain and land-use are not representative of higher-resolution values affecting the anemometer measurement. For example, Meridian, Mississippi lies in a narrow valley that is oriented north-to-south (Figure 2.2). The valley causes observed winds to be funneled primarily from the north or south directions. The 2.5' latitude-longitude model elevation, however, does not resolve the narrow valley very well. This causes modeled surface winds to be controlled by larger topographic features and upper level conditions, such as in May, when modeled wind directions prevail from the southwest. While absolute differences between modeled and observed winds at Meridian show only small speed differences there is a frequent directional bias of 15 to 30 degrees in May, likely caused by the differences between actual and model topography.

In general, the model performed very well with respect to both wind speed and wind direction. The two land-use categories (land and water) in the model, however, tend to bias rough terrain (forested and mountainous). This causes strong winds (> 8 m/s) to be underestimated over broad flat areas and grass lands. Also, the smoothed model terrain appears to cause a modest directional bias of less than 45° in either the clockwise or counterclockwise direction. Finally, restrictions on the model lapse rate (temperature difference with height) and lack of radiative heating appear to cause poor model performance in some months at western arid sites.

## 2.2 Overlap Domains

The hydrostatic assumption and other simplifying physics cause the numerical processing in WINFLO to have difficulty converging to a solution when there is a sharp pressure ridge or trough in the modeling domain. To maximize convergence opportunities, we divided the country into overlapping regional domains (Figure 2.3). Each domain was selected to encompass terrain features that may influence pressure-gradient forces and minimize potential edge effects. Because numerical results never yield exactly the same value, we merged model runs from overlapping domains with a simple weighted-average algorithm. The scheme used weights proportional to the distance from the boundary of the domain. A grid cell on the boundary receives a weight of zero, a grid one cell away from the boundary receives a weight of one, and so on. Wind speed and direction were averaged separately then combined to give the final wind vector. Wind speed was averaged as a typical weighted mean. To calculate the average wind direction, weighted means were found for the cosine (east-west) and sine (north-south) components of the wind direction. The resulting direction is the arctangent of the mean north-south component divided by the mean east-west component. For example, if a specific grid cell in an overlap region was located 17 grid cells from the edge of the Northwest domain with a speed of 3.0 m/s from 180° and 75 grid cells of the edge of the Northern Rockies domain with a speed of 3.5 m/s from 170°, its resulting speed value would be 3.4 m/s  $[(3 \times 17) + (3.5 \times 75)] / (17 + 75)$  and its resulting direction value would be 171.8° or:

$$W_s = \frac{(3.0 \times 17) + (3.5 \times 75)}{(17 + 75)} = 3.41 \text{ m/s}$$

$$W_d = \arctan \left[ \frac{(\sin 180^\circ \times 17) + (\sin 170^\circ \times 75)}{(\cos 180^\circ \times 17) + (\cos 170^\circ \times 75)} \right] = 171.8^\circ$$

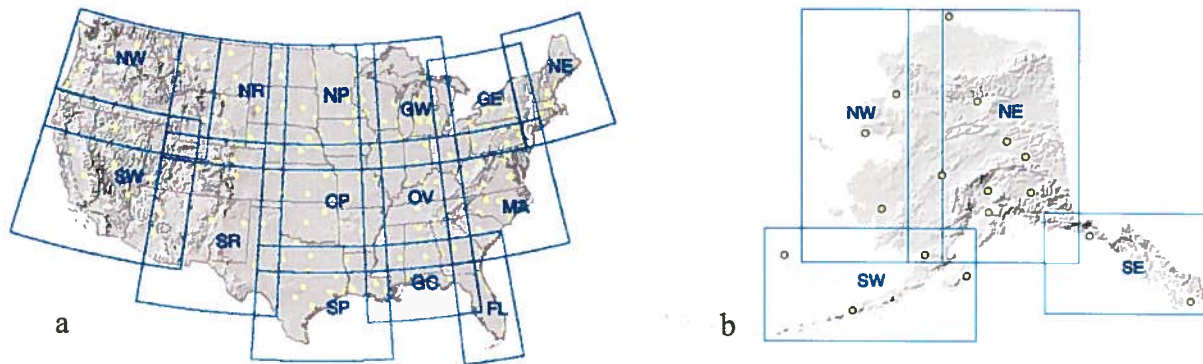


**Figure 2.3.** Domains used for modeling surface wind in (a) the contiguous 48 states and (b) Alaska. Hawaii was modeled in a single domain. Dots indicate places with available observations that were used for verification.

While the small domains helped reduce the amount of missing wind values, there still were times when the model did not converge. Table 2.2 summarizes the percent of time that WINFLO failed to converge in each domain for each month. This indicates the number of times wind data were not generated and unavailable for ventilation index calculations. WINFLO clearly had the most difficult time in the Mid Atlantic and New England regions during the winter. This may be due to the vigorous storms that can occur in those regions and the difficulty of convergence when there are steep gradients in the pressure field. Also, there is some indication that WINFLO has difficulty with storms moving into the domain from the east (P. Speers, personal communication 1999), which is possible on the eastern seaboard.

**Table 2.2.** Percent of missing wind data for each modeling domain of the contiguous 48 states.

Domain	Jan	Feb	Mar	Apr	May	Jun	Jul	Aug	Sep	Oct	Nov	Dec	Total
Central Plains	0.38%	0.25%	0.13%	0.08%	0.00%	0.00%	0.00%	0.00%	0.00%	0.00%	0.00%	0.08%	0.93%
Florida	7.00%	7.09%	5.99%	4.14%	1.01%	0.42%	0.00%	0.00%	0.34%	1.05%	3.21%	5.27%	35.53%
Great Lakes East	2.32%	2.24%	1.77%	0.89%	0.76%	0.17%	0.04%	0.13%	0.25%	0.25%	0.93%	2.11%	11.86%
Great Lakes West	7.09%	5.32%	3.76%	3.50%	2.32%	1.05%	0.34%	0.42%	1.22%	1.69%	3.08%	4.81%	34.60%
Gulf Coast	1.81%	2.36%	1.22%	0.76%	0.30%	0.08%	0.00%	0.00%	0.00%	0.25%	0.97%	1.77%	9.54%
Mid Atlantic	12.83%	12.66%	11.01%	6.67%	5.15%	2.19%	0.84%	0.80%	0.84%	3.00%	4.77%	9.62%	70.38%
New England	11.39%	11.14%	10.51%	9.66%	7.26%	2.45%	1.18%	1.31%	5.32%	5.40%	7.09%	8.95%	81.65%
Northern Plains	0.80%	0.72%	0.13%	0.08%	0.00%	0.00%	0.00%	0.00%	0.00%	0.04%	0.08%	0.46%	2.32%
North Rockies	1.56%	0.84%	0.38%	0.00%	0.00%	0.00%	0.00%	0.00%	0.00%	0.04%	0.25%	0.72%	3.80%
Northwest	0.84%	0.30%	0.21%	0.08%	0.00%	0.00%	0.00%	0.00%	0.04%	0.13%	0.80%	0.30%	2.70%
Ohio Valley	0.17%	0.13%	0.08%	0.08%	0.00%	0.00%	0.00%	0.00%	0.00%	0.00%	0.00%	0.08%	0.55%
Southern Plains	0.97%	1.05%	0.59%	0.25%	0.08%	0.00%	0.00%	0.00%	0.00%	0.04%	0.30%	1.22%	4.51%
South Rockies	0.17%	0.13%	0.04%	0.04%	0.00%	0.00%	0.00%	0.00%	0.00%	0.00%	0.00%	0.08%	0.46%
Southwest	0.00%	0.04%	0.00%	0.00%	0.00%	0.00%	0.00%	0.00%	0.00%	0.00%	0.00%	0.00%	0.04%
All Domains	47.34%	44.26%	35.82%	26.24%	16.88%	6.37%	2.41%	2.66%	8.02%	11.90%	21.48%	35.49%	258.86%

Because several domains were merged together to generate a national coverage of wind we closely examined winds in the overlap regions to evaluate potential edge effects. In all cases, we found model-generated winds from one domain to be reasonably consistent with winds generated from the overlapping domain. For example, Medford, Oregon and Winnemucca, Nevada are two stations in the overlap zone between the Northwest and Southwest domains, with Winnemucca near the center of the overlap zone and Medford near the northern border of the Southwest domain. The two model runs agree more closely at the central site (Winnemucca) but do not differ grossly at the border site (Medford) (Figure 2.4). Because data near the border of a domain receives less weight when the domains are merged, the edge effect becomes negligible in the merged data.

Observations in each overlap domain were used to check for consistency between model output from individual domain runs and calculated overlap values. In general, no accuracy was lost by employing the overlap merging algorithm and realistic national patterns of wind resulted.

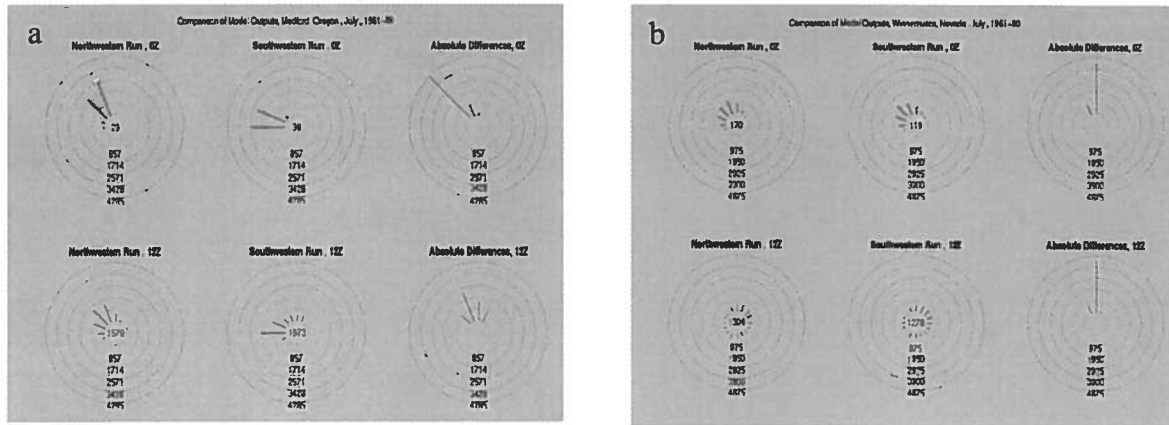


Figure 2.4. Absolute differences between modeled winds as derived from the Northwestern and Southwestern domains at a) Medford, Oregon and b) Winnemucca, Nevada.

## 2.3 WINFLO-XY for Alaska

The numerical routines in WINFLO assume relatively square grid cells even though it is based on latitude-longitude coordinates. This assumption appears to work well in mid-latitudes, where the model has been most successfully employed, but is not valid in upper-latitude regions, above about the 52nd parallel, such as Alaska. We created a constant distance version of WINFLO (WINFLO-XY) to apply in the Alaskan region and ensured that it produces similar results to the original WINFLO in mid-latitudes. Whereas the conterminous 48 states and Hawaii have grid resolutions of 2.5° latitude-longitude, which is about 5 km, the Alaskan grid cells are fixed at 5 km on a side. Digital elevation model (DEM) data were aggregated and projected (see Appendix 1) to match the grid size in each domain, providing the lower boundary of WINFLO.

## 2.4 Key Elements of Wind

- The WINFLO surface wind model is computationally efficient, reasonably accurate, and has shown success in a variety of applications.
- Surface winds apply to conditions near sunrise (1200 UTC) and sunset (0000 UTC).
- Surface winds over broad flat areas and grasslands may be underestimated at times.
- Gusty surface winds may be underestimated by the WINFLO but the model successfully simulates strong, sustained storm winds.
- The choice of the 85 kPa (about 1500 m asl) height as an upper initialization field appears reasonable, even over high-elevation mountains.
- Surface wind speeds from WINFLO are consistently slower than observed, especially during the afternoon in spring and summer.

- WINFLO performs with similar accuracy to MM5, a fully physical, 3-dimensional, non-hydrostatic model.
- Differences between model and observed wind values do not necessarily indicate error. Modeled values represent conditions over a smoothly varying surface while observations indicate conditions at a point in a rough landscape.
- Comparison plots of model and observed winds for all locations in the observation database can be found on the VCIS web site at <http://www.fs.fed.us/pnw/fera/vent>.
- Merging several subdomains generated a nationally consistent database of wind.

### 3.0 MIXING HEIGHT

Because the NCEP Reanalysis data are at a relatively coarse vertical resolution, mixing heights are determined from radiosonde observation (RAOBS) data. To derive mixing heights, we lift a parcel of air adiabatically from the surface with a starting temperature near the maximum or minimum daily temperature as described in Holzworth (1972). The mixing height is defined as that level where the temperature of the adiabatically lifted parcel becomes less than the measured ambient temperature. Once this occurs, it is assumed that the parcel, being cooler than its surroundings, will sink back toward the surface.

The calculated mixing heights are interpolated between radiosonde observation sites (Fig. 3.1) using the Cressman scheme (1959) as described in (Manning and Haagenson 1992). Frontal boundaries between air masses are not considered, partly because they are difficult to determine automatically from archived data, and also because we assume that their exact position is not critical in a climatological assessment of mixing height. Thus mixing height is mapped to smoothly vary over the landscape except on calm, clear nights when the morning mixing height is modified by an inversion potential algorithm that identifies basins and valleys where cold air and smoke may accumulate.

#### 3.1 Mixing Height Verification

We used a standard method of deriving mixing height. Because we used coincident surface observations instead of maximum and minimum, however, we chose to verify our methods against mixing heights derived by the Environmental Protection Agency (United States EPA 2001) for the years 1984 to 1990. At each radiosonde location we created scatter diagrams of mixing heights to help highlight differences. Figure 3.2 shows an example from Pittsburgh, Pennsylvania. Points falling on the diagonal indicate perfect agreement. Most values agree quite well. Significant differences arise for missing data (solid blue triangles). Our missing values were omitted and were different than EPA missing values, which were filled. Differences also occur for temperature change values (open greentriangles). EPA adjusted values when the selected temperature values were less than the 1200 UTC RAOB temperature while we made no adjustments.

Two sites, Omaha, Nebraska and Corpus Christi, Texas show significant differences in all values (Fig. 3.3). We are investigating the cause of these discrepancies. Until we isolate and fix the cause, mixing-height values in regions around these sites should be used cautiously.

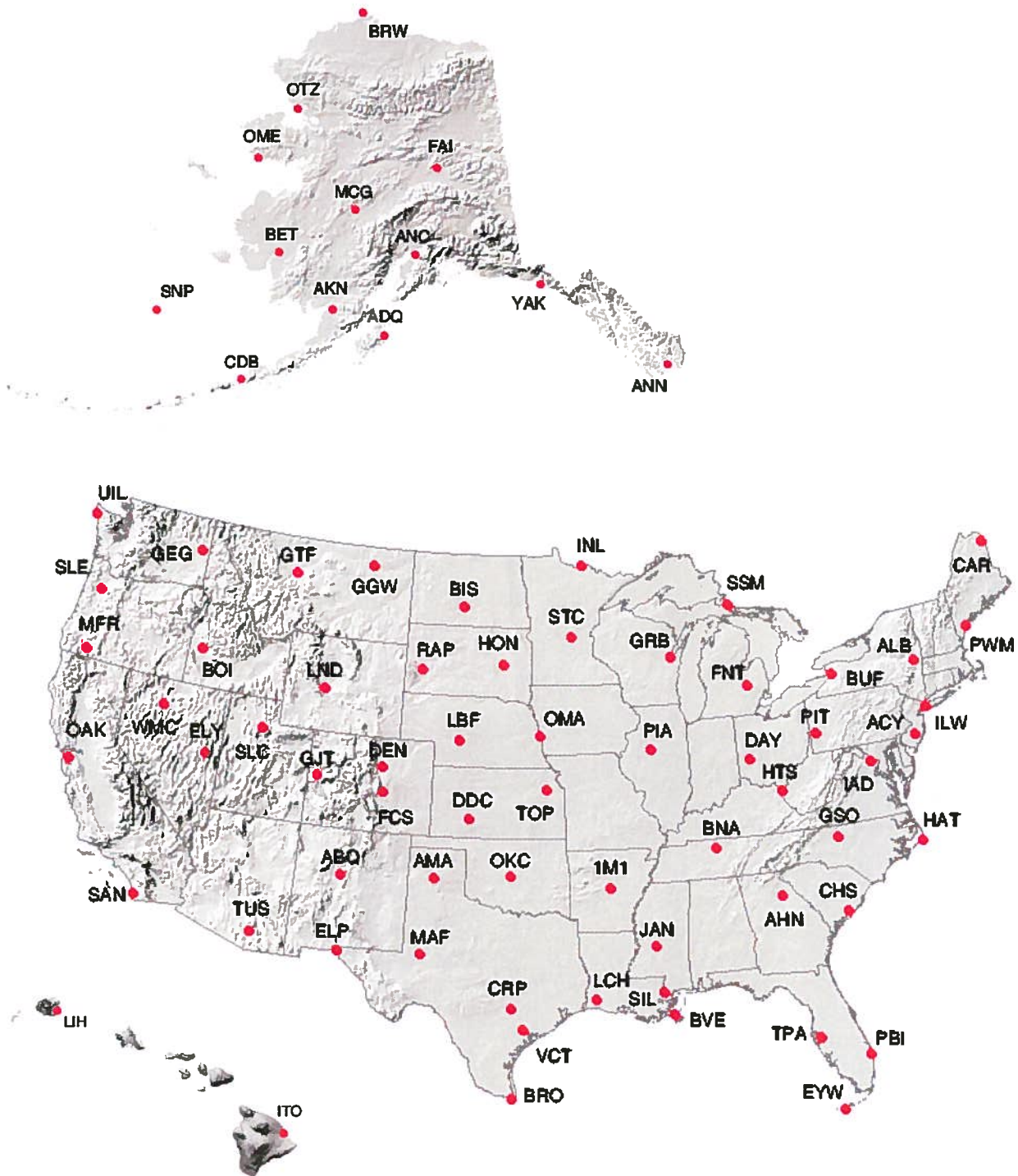


**Figure 3.1.** Available radiosonde locations used to calculate mixing height in the contiguous United States, Alaska, and Hawaii.

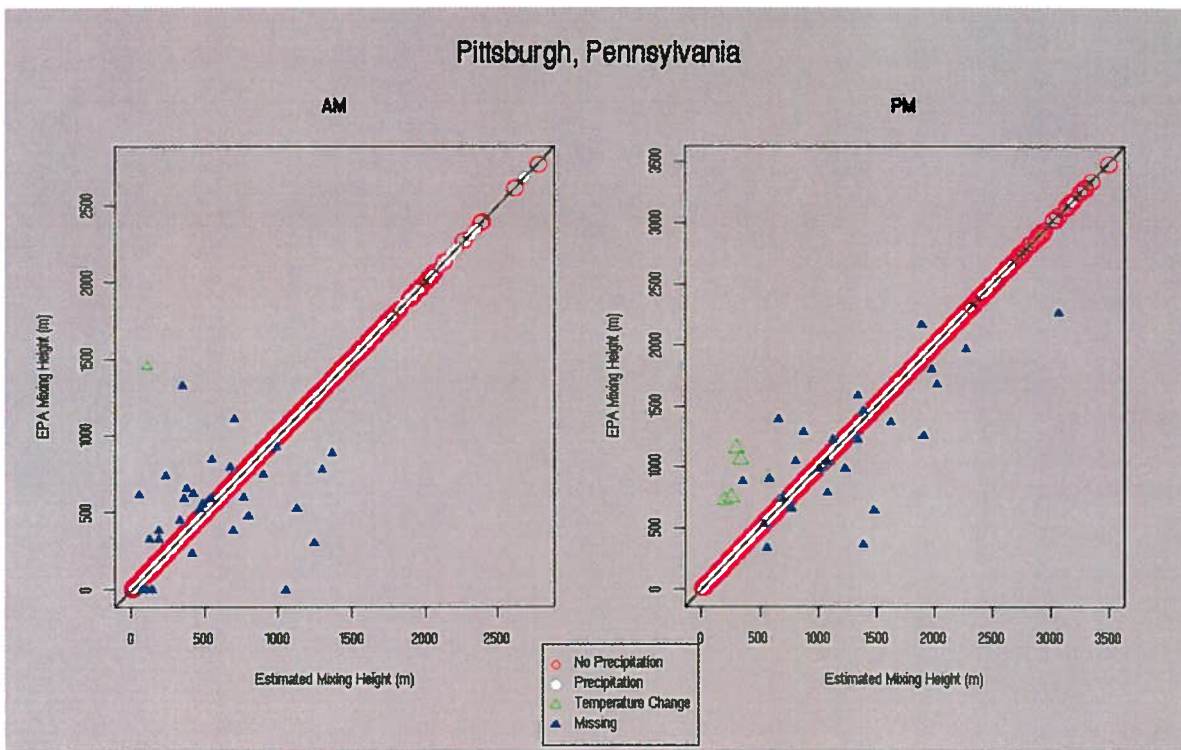


**Figure 3.2.** Mixing heights calculated by EPA vs. VCIS data for morning (AM) and afternoon (PM). Only data that differ by more than 5 meters are shown. Values are shown for days with no precipitation (open red circles), with precipitation (solid white circles), when a temperature change occurred (open green triangle), and when missing data were estimated in the EPA algorithm (solid blue triangles).

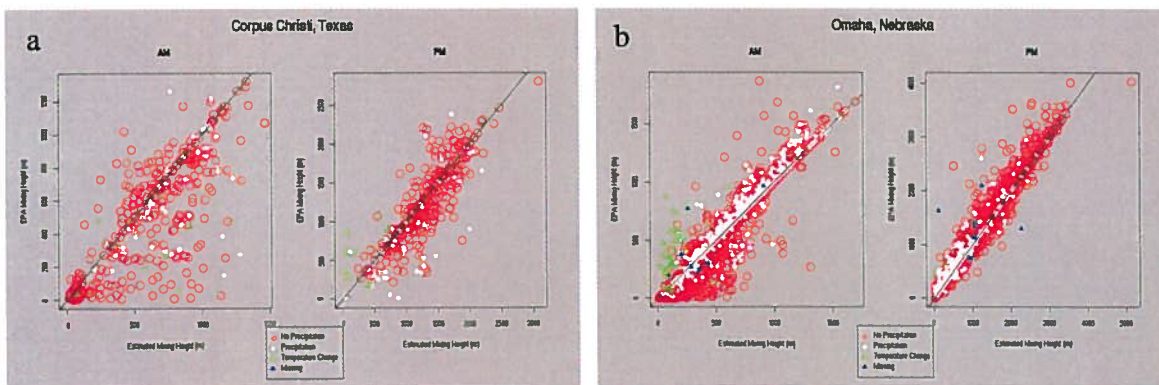


**Figure 3.3.** Mixing heights calculated by EPA vs. VCIS data for morning (AM) and afternoon (PM) in (a) Corpus Christi, Texas and (b) Omaha, Nebraska. See Figure 3.2 for a description of symbols.

## 3.2 Local Inversion Potential

At night, in addition to the stabilization of air and decreased mixing height, downslope winds and terrain features can cause cooling air to be trapped in stagnant pools forming patterns of local temperature inversions in places well away from and poorly represented by RAOBS. These areas also can trap smoke and other pollutants. Currently there is no meteorological model that can adequately simulate the timing and location of local inversions on a national scale. Therefore, we created a set of algorithms that determine the occurrence, location, and strength of local temperature inversions based climate records of nearby surface weather stations and terrain features.

### 3.2.1 Local Inversion Occurrence

To determine the occurrence potential of a local inversion, a set of criteria were adapted from Pasquill (1962) and Turner (1964) who describe the formation of a surface-based temperature inversion as dependent on the surface wind speed and the net longwave radiation leaving the lowest layer of the atmosphere, which depends on cloud cover. Hourly values of wind speed, total cloud cover, opaque cloud cover, and present weather (defined as fog, drizzle, rain, snow, etc.) (National Renewable Laboratory 1992; National Climatic Data Center 1997) are used to determine whether a stable surface layer will form. Inversion occurrence potential is defined to occur if the following criteria are met for at least 50% of all reported hours between 1800 and 0600 local time:

- Wind speed is  $\leq 3$  m/s, total cloud cover is  $\leq 8/10$ , and opaque cloud cover is  $\leq 6/10$ , or
- wind speed is  $> 3$  m/s but  $\leq 5$  m/s, the total cloud cover is  $\leq 6/10$  and opaque cloud cover is  $\leq 3/10$ ; or
- if fog has been reported at any hour between 1800 and 0600 local time.



**Figure 3.4** Local occurrence neighborhoods for determining inversion potential. Letters indicate NWS identifier for the station that was used to determine calm, clear conditions within the neighborhood.

On nights with excessive missing data, no inversion is expected if there are more than two reports of winds exceeding 5 m/s. If all reported winds are less than 5 m/s, then the available hours of cloud cover determine inversion potential.

Criteria for the occurrence of a local inversion were checked at all available surface stations then applied to grid cells in the surrounding nearest neighbors. If a surface-based inversion were determined to occur at the observing station then all grid cells within the neighborhood also were assumed to have a local inversion potential. Figure 3.4 shows how neighborhoods are spaced in the contiguous 48 states and Alaska. Local inversion potential was not determined in Hawaii because the 2.5' latitude/longitude grid resolution could not resolve island valleys.

### 3.2.2 Local Inversion Location

To locate and rank potential local inversions, a GIS algorithm was developed to identify terrain features that promote the collection and trapping of subsiding air, following initial suggestions from Dr. Jan Henderson (USDA Forest Service, Region 6). An area centered over the intermountain region of the United States is used as an example of how local inversion potential is determined on a 5-km modeling grid with the following steps:

1. Height is vertically exaggerated by 5 times (Figure 3.5). This helps to highlight shallow **valleys and hollows** that are difficult to resolve with 5-km grid cells.

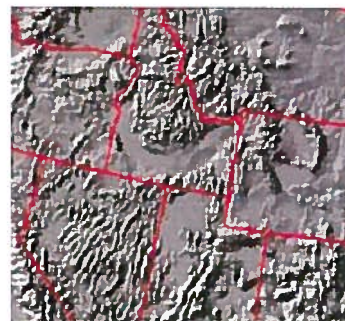


Figure 3.5. Domain over inter-mountain region of the U.S. with height exaggerated by 5 times.

2. **Flat areas** are defined by slope that is less than  $0.8^\circ$  and, to eliminate insignificant flat areas, a 3 pixel  $\times$  3 pixel smoothing filter is applied (Figure 3.6).



Figure 3.6. Slope  $< 0.8^\circ$  after 3x3 smoothing filter.

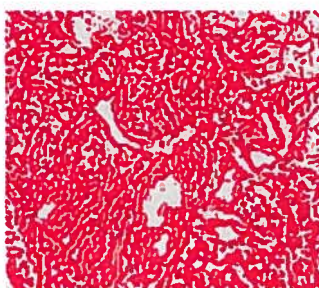


Figure 3.7. Negative curvature after 1-cell radial filter.

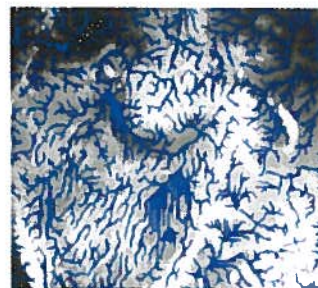


Figure 3.8. Flow accumulation from at least 17 pixels.

3. **Valleys and basins** are defined by negative curvature, which is smoothed with a one-cell radial filter (Fig. 3.7).

4. **Flow accumulation** is computed for areas exceeding 17 pixels (Fig. 3.8). The 17-pixel threshold is chosen subjectively to eliminate flow potential that crosses ridgelines or begins at mountaintops. With a 5-km grid size, the threshold is  $425 \text{ km}^2$ .

5. Because not all places of negative curvature (e.g., benches) will form a local inversion, potential areas of drainage accumulation are defined by places where lines of **flow accumulation intersect valleys and basins**.

6. Because not all flat places will form a local inversion (e.g., plateaus), potential areas of pooling are defined by places where lines of **flow accumulation intersect flat areas**.

The resulting map of potential inversion locations in the example domain is shown in Fig. 3.9.



**Figure 3.9.** Result of inter-secting flow accumulation with flat areas and valleys and basins.

### 3.2.3 Local Inversion Strength

We derived values of strength to help map inversion heights by assuming that the potential strength of local inversions is correlated to the amount of accumulated flow. In general, as flow accumulation increases downstream, so does the inversion strength. Strength values increase rapidly as rivers join and when flow is contributed from different watersheds. By superimposing flow accumulation on the inversion potential map, we derived inversion strength values that ranged from 0 to 11589, with over 95% of the grid cells having a value less than or equal to 366.

To determine the height above ground, we applied a logarithmic function:

$$H = 25.2430 \times \log_e [S_i \times 1.0404],$$

where  $H$  is the inversion height in meters above ground level (agl) and  $S_i$  is the inversion strength truncated below 366. By bounding the inversion strength values below 366 (i.e., all values above 366 were given a value of 366) we could keep the inversion height from exceeding 150 m agl, the typical height of nighttime surface-based inversions.<sup>5</sup>



**Figure 3.10.** Inversion location and relative depth with red colors indicating maximum flow accumulation with depths near 150 m a.g.l and blue colors with minimum flow accumulation. White indicates places where local inversions are not expected to form.

The vast majority of major valleys have inversion strengths less than 366. For example, the Bitterroot Valley in Montana has an inversion strength of about 40, giving it an inversion height of 94 m agl at the valley bottom. The Snake River Valley in Idaho and the mouth of the Columbia River in Oregon have inversion strengths of about 618 and 7000, respectively. Because both are greater than 366, their potential inversion height at valley bottom is 150 m a.g.l. Note that inversion heights decrease toward the head of the valley. This allows a somewhat smooth transition between areas with a local inversion and areas without a local inversion.

<sup>5</sup> Holzworth and Fisher (1979) found that nearly all surface-based inversions were at least 100 m deep.

### 3.2 Local Inversion Verification

There are very few direct observations of local inversion occurrence or location. At RAOB locations, where surface-based inversions can be directly measured, we tested our inversion occurrence criteria and found that observed surface-based inversions occurred on nearly all days that the criteria of calm wind and clear skies were met. A surface-based inversion was determined to exist if the 1200 UTC

**Table 3.1.** Comparison between observed inversion from raob and predicted inversion from nighttime surface weather. "P" scores associated with chi-squared tests are shown for each observation location and each month. White = no relationship, tan = significant relationship ( $p < 0.05$ ), red = highly significant relationship ( $p < 0.01$ ). Column headings represent RAOB site names whose locations can be found in Figure 3.1.

	ABQ	ALB	AHN	BIS	BRO	CAR	DAY	DDC	ELP	ELY	FNT	GGW
Jan	0.130	0.101	0.036	0.014	0.040	0.132	0.068	0.205	0.016	0.268	0.141	0.101
Feb	0.060	0.033	0.018	0.013	0.006	0.114	0.029	0.059	0.063	0.370	0.022	0.041
Mar	0.012	0.011	0.003	0.021	0.002	0.101	0.015	0.029	0.017	0.104	0.034	0.049
Apr	0.026	0.056	0.013	0.007	0.009	0.127	0.018	0.064	0.020	0.086	0.021	0.049
May	0.097	0.225	0.004	0.020	0.011	0.381	0.012	0.026	0.032	0.103	0.025	0.029
Jun	0.084	0.403	0.015	0.042	0.008	0.372	0.024	0.074	0.155	0.163	0.021	0.104
Jul	0.158	0.442	0.057	0.005	0.038	0.257	0.020	0.222	0.061	0.433	0.045	0.083
Aug	0.066	0.066	0.015	0.043	0.043	0.076	0.012	0.205	0.024	1.000	0.006	0.172
Sep	0.012	0.011	0.004	0.003	0.004	0.061	0.002	0.010	0.032	0.251	0.001	0.080
Oct	0.005	0.032	0.003	0.007	0.007	0.066	0.002	0.023	0.041	0.272	0.003	0.003
Nov	0.016	0.035	0.006	0.011	0.014	0.101	0.014	0.011	0.008	0.107	0.018	0.043
Dec	0.018	0.190	0.008	0.009	0.001	0.215	0.174	0.205	0.007	0.130	0.069	0.046

	GJT	GTF	GRB	GSO	HTS	INL	LND	MFR	MAF	LBF	PIA	PIT
Jan	0.072	0.548	0.064	0.017	0.014	0.045	0.031	0.100	0.035	0.014	0.046	0.068
Feb	0.174	0.545	0.011	0.008	0.037	0.004	0.054	0.020	0.020	0.013	0.103	0.060
Mar	0.113	0.154	0.019	0.002	0.007	0.002	0.011	0.011	0.043	0.007	0.035	0.006
Apr	0.080	0.071	0.021	0.019	0.023	0.011	0.015	0.007	0.049	0.003	0.042	0.007
May	0.113	0.203	0.009	0.029	0.021	0.007	0.035	0.006	0.020	0.011	0.017	0.024
Jun	0.184	0.193	0.021	0.010	0.020	0.021	0.056	0.001	0.109	0.010	0.014	0.057
Jul	0.190	0.148	0.017	0.008	0.061	0.011	0.272	0.020	0.050	0.094	0.068	0.020
Aug	0.360	0.148	0.009	0.021	0.024	0.017	0.241	0.002	0.018	0.031	0.038	0.017
Sep	0.141	0.020	0.005	0.004	0.029	0.006	0.009	0.004	0.008	0.014	0.012	0.010
Oct	0.049	0.145	0.008	0.006	0.023	0.008	0.008	0.001	0.001	0.004	0.014	0.007
Nov	0.184	0.553	0.012	0.009	0.008	0.029	0.047	0.102	0.006	0.004	0.017	0.012
Dec	0.138	0.548	0.078	0.021	0.020	0.018	0.027	0.019	0.006	0.002	0.011	0.022

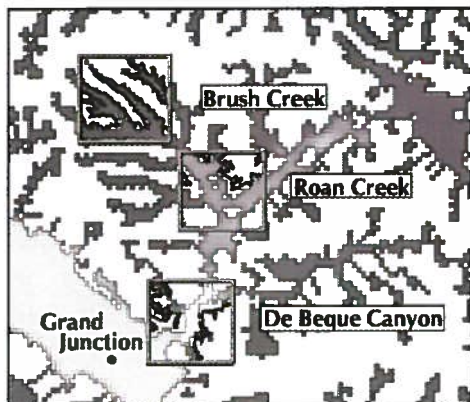
	PWM	UIL	RAP	STC	SLE	SLC	GEG	IAD	TOP	TUS	WMC	YAK
Jan	0.053	0.064	0.017	0.029	0.080	0.049	0.169	0.032	0.060	0.042	0.042	0.142
Feb	0.047	0.029	0.004	0.240	0.011	0.107	0.088	0.018	0.018	0.058	0.165	0.075
Mar	0.029	0.006	0.001	0.050	0.003	0.047	0.020	0.018	0.008	0.019	0.031	0.030
Apr	0.027	0.004	0.003	0.026	0.003	0.049	0.008	0.019	0.001	0.031	0.031	0.029
May	0.139	0.004	0.024	0.008	0.008	0.024	0.007	0.033	0.007	0.113	0.061	0.061
Jun	0.466	0.004	0.083	0.103	0.002	0.042	0.009	0.135	0.026	0.159	0.126	0.042
Jul	0.269	0.001	0.137	0.092	0.006	0.037	0.012	0.031	0.052	0.141	0.147	0.037
Aug	0.074	0.007	0.047	0.038	0.002	0.083	0.006	0.046	0.017	0.113	0.406	0.023
Sep	0.001	0.002	0.004	0.016	0.020	0.009	0.007	0.009	0.007	0.287	0.094	0.071
Oct	0.014	0.003	0.011	0.009	0.003	0.059	0.013	0.011	0.001	0.159	0.043	0.066
Nov	0.032	0.035	0.004	0.007	0.045	0.024	0.080	0.017	0.003	0.128	0.030	0.066
Dec	0.036	0.031	0.015	0.021	0.001	0.020	0.082	0.020	0.003	0.087	0.083	0.068

RAOB included two adjacent layers within 1000 meters of the surface that reported warmer air over cooler air. No distinction was made between inversion strength or depth. The resolution of the temperature data is to the nearest tenth of a degree centigrade.

Table 3.1 shows “p values” associated with chi-squared tests for each month. A  $p$ -value less than 0.05 indicates a strong relationship or agreement between the RAOB observed inversion and the surface-based algorithm. The table is color coded to show areas of no relationship (white), significant relationship ( $p < 0.05$ ), and highly significant relationship ( $p < 0.01$ ).

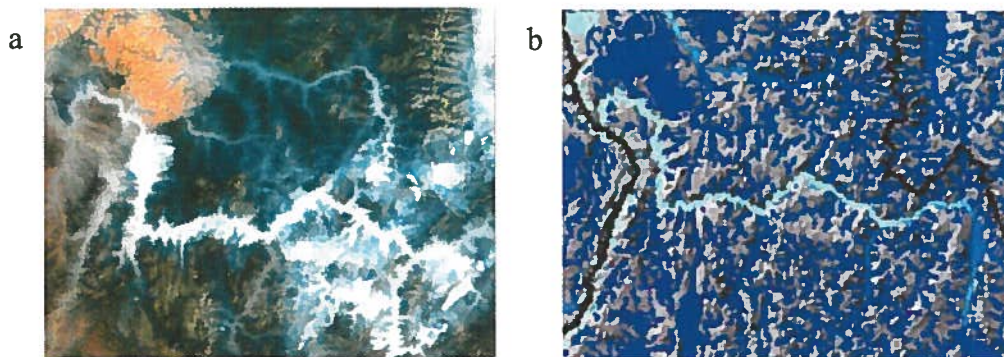
Inversion occurrence is determined from radiosonde observations (RAOBS), which are sparsely distributed over the United States. Additionally, these stations are typically located in flat areas or broad valleys where local inversions are less significant than in narrow valleys, small hollows, and basins that are typical of wildland areas. Therefore, most of our verification techniques for local inversion potential are qualitative in nature.

Figure 3.11 shows local inversion potential compared to measurements from the ASCOT experiments in central Colorado (Neff and King 1989). The solid black lines mark elevations at the height of an observed inversion. Gray shades indicate potential inversion derived from terrain features.



**Figure 3.11.** A map of local inversion potential locations (gray shades) shown with inversion height observations (black lines) in central Colorado.

Another way to check the reasonableness of the terrain algorithm is to compare maps of local inversion potential with satellite observations. Figure 3.12a shows a MODIS satellite image over the Salmon River in central Idaho during the 2000 wildfires and a map of local inversion potential for the same general area is shown in Figure 3.12b. Inversion potential is shaded with light blue being the strongest potential. From the satellite image, it appears that most smoke is concentrated in the Salmon River valley, where the strongest inversion potential is indicated. Darker blue colors indicate potential inversions in side valley and tributaries, just as they appear in the satellite image.



**Figure 3.12.** (a) Observations of smoke over central Idaho at about 10am in July 2000. (b) Map of inversion potential with light blue showing strongest potential and dark blue showing weaker potential.

### 3.4 Adjusted Mixing Height

The local inversion algorithm was applied to morning (1200 UTC) mixing heights only and only to grid cells in the neighborhood of a surface observation showing calm winds and clear skies the previous night. Grid cells not in a terrain feature that fosters the development of a local, nighttime inversion (i.e., peaks, ridges, plateaus, etc.) are assumed to be experiencing the ambient condition of mixing heights interpolated from RAOB measurements.

Figure 3.13 shows how mixing height patterns change on a July morning when the local inversion potential is imposed. Note that valley inversions become visible in the northwestern United States and in the Appalachian Mountains after the inversion algorithm is imposed. Also note a sharp

discontinuity in Florida where Tampa, in west-central Florida, did not experience calm, clear nighttime conditions while adjacent neighborhoods did, forcing the local inversion throughout Florida except in grid cells surrounding Tampa.

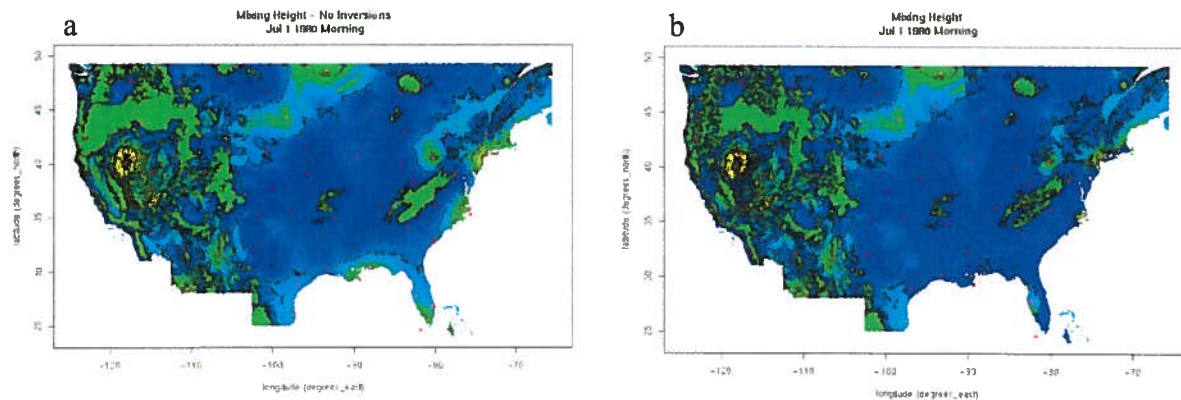


**Figure 3.13.** Interpolated mixing height for the morning of July 1, 1980 (a) without adjustment for local inversion, and b) with local inversions. Blue colors indicate lowest heights and green colors indicate highest heights.

There are times when the measured mixing height passes below ground level as it is interpolated across the landscape. This happens frequently when the mixing height is relatively low, such as during a winter morning, or in places where mountains are between RAOB locations. At these times and in these places, above the interpolated mixing height, the air parcels often are free to lift to great heights, occasionally reaching the tropopause.<sup>6</sup> While RAOB measurements can help locate the height of parcel trajectories above the mixed layer, computations were too cumbersome to employ in this application. Therefore, we arbitrarily assigned a mixing height, or “free” height, to places where the interpolated mixing height values were at ground or below ground level. In the afternoon, we set the “free” height to be 4000 m agl, which is about the highest measured afternoon mixing height, and the morning “free” height is set at 1000 m agl, which is about the highest measured morning mixing height (Holzworth 1972). The best way to view the effect of this imposed “free” height is to view time-series statistics of mixing height at individual points, which are available on the VCIS web site [www.fs.fed.us/pnw/fera/vent](http://www.fs.fed.us/pnw/fera/vent). The time-series are designed as box plots so the user can determine how common a certain mixing height may be at any selected point. Each box plot include a red line at the imposed “free” height level to help determine the frequency of times that observed mixing heights were mapped below terrain at any point on the landscape. Appendix 2 provides examples and describes how to interpret time-series box plots for VCIS mixing height.

Figure 3.14 shows the effect of adjusted mixing heights. In **A**, the observed mixing height is mapped below ground level. While parcels of air at points *a*, *e*, and *g* ventilate in response to the observed mixing height, parcels originating from places above this layer will ventilate through a deeper layer of the atmosphere. Air parcels originating in basins or valleys that exhibit a potential for local inversion, such as at points *c* and *f*, will be trapped to elevations below 150 m agl. In **B**, the observed mixing

<sup>6</sup> The tropopause marks the boundary between the troposphere, where temperature generally decreases with height, and the stratosphere, where temperature generally increases with height. The tropopause is about 7,000 m asl in the polar regions, about 10,000 m asl in the mid latitudes, and about 17,000 m asl in the tropics.

height is mapped above ground level everywhere. The ventilation of air parcels originating from anywhere except in places with local inversions (points *c* and *f*) will respond to the height of the observed mixing layer. In this case, smoke plumes originating from points *a*, *e*, and *g* may loft to higher elevations than in **A** when observed mixing heights are lower. But plumes originating from points *b* and *d* may not be ventilated as well as in **A** because the observed mixing height is lower than an imposed “free” height.

Note that the tropopause or an inversion layer in the upper atmosphere that limits mixing will be nearly horizontal relative to sea level but may bend gradually over higher terrain, such as the Rocky Mountains. While it is somewhat unrealistic to force the “free” height to follow terrain heights, it appears to be an adequate approximation. Also, fixing a height above ground level was the most computationally efficient way to create a positive mixing height value and does not seem to seriously compromise the physical reasonableness of resulting mixing height patterns. Clearly, more rigorous methods of deriving “free” heights are needed.

It also should be noted that during winter, patterns illustrated in Figure 3.14A are common where observed mixing heights are somewhat low and map below high terrain, while in summer, patterns illustrated in Figure 3.14B are common where observed mixing heights are relatively high and map to elevations just above high terrain. This affects the seasonal distribution of mixing height values in high terrain, causing winter mixing heights to appear higher than summer mixing heights. While seemingly contrary to intuition, it is not unreasonable.

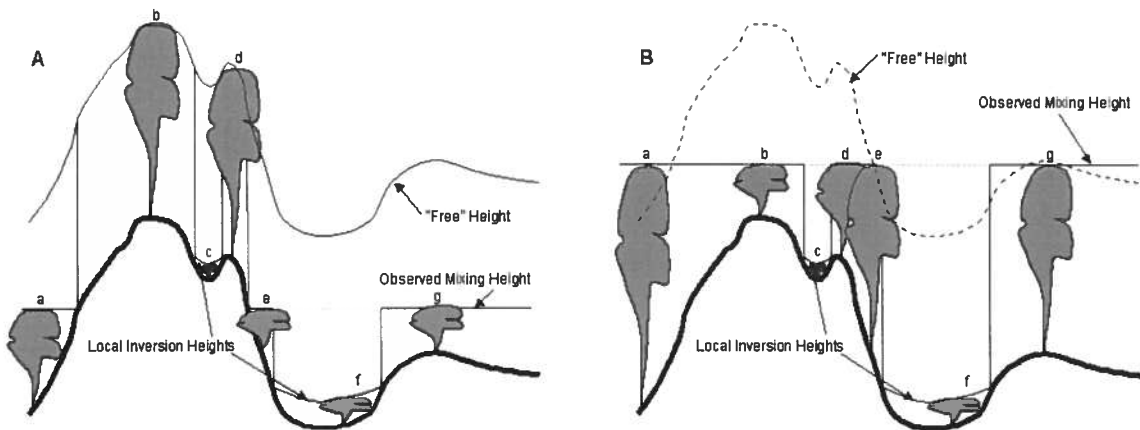


**Figure 3.14.** Schematic diagram of adjustments to the mixing height in areas of complex terrain. The observed mixing height is interpolated between RAOB measurements; local inversion heights are determined by the amount of down-slope flow accumulation and invoked only on mornings following calm, clear nights; the “free” height is arbitrarily set at 4000 m agl during the afternoon and 1000 m agl in the morning. Gray clouds indicate potential vertical mixing for **A**) when observed mixing height is mapped below ground level in places, and **B**) when observed mixing height is mapped above ground level.

### 3.5 Key Elements of Mixing Height

- Mixing heights were calculated from RAOB measurements using a standard parcel method.
- At high-elevation locations it may appear that the VCIS mixing height is higher during winter than summer.
- Values of mixing height are generally consistent with EPA-derived values.
- Morning mixing heights are adjusted to account for local, surface-based inversions that are common in valleys and basins at night.
- Local inversion potential is applied only to grid cells in the neighborhood of a surface observation site showing calm, clear conditions at night.
- Local inversion potential is applied only to grid cells within terrain features that foster the formation of the development of a nighttime inversion. The height of a local inversion is capped at 150 m agl and determined by the amount of potentially accumulating nighttime drainage flow.
- Surface observations of wind and cloud cover can correctly predict the occurrence of a local, surface-based inversion most of the time.
- An algorithm based on terrain features can correctly predict the location of a local inversion most of the time.
- Discontinuities in mapped values of morning mixing height occur when adjacent surface observation stations experience different nighttime conditions, causing the local inversion algorithm to be invoked in one neighborhood and not in the other.
- When observed mixing heights are mapped at or below ground level, an arbitrary height of 4000 m agl in the afternoon or 1000 m agl in the morning is imposed.

### 4.0 VENTILATION INDEX

The ventilation index has become a useful tool for air pollution management throughout the United States. Fire and smoke managers in the southeastern United States are most familiar with using a ventilation index and several states use the index, sometimes called a clearing index, to help regulate outdoor burning (Hardy and others 2002). While popular as an assessment and prediction tool, heretofore there has been no historical review of ventilation potential. This has prevented an understanding of the spatial and temporal variability of ventilation and its associated impact on values of air quality and visibility.

**Table 4.1.** Classification of ventilation potential from ventilation index values in the VCIS database.

Ventilation Index (m <sup>2</sup> /s)	Classification
0-1175	Poor
1176-2350	Marginal
2351-3525	Fair
>3525	Good

The ventilation index is the product of wind speed and mixing height. In most cases, the index uses the average value of wind speed in the mixed layer or a local steering wind, which often is well above 10 meters, the height of wind derived for this study. Also, we have modified the mixing height to

account for local inversions. The local inversion correction creates lower values of ventilation potential at remote sites, which is more applicable than indexes calculated from a central RAOB location. Therefore, values of ventilation index in VCIS are relatively conservative and may best be applied to smoke concerns relatively close to the ground.

To map the index values in a meaningful way and help assess the values of air quality and visibility that are at risk from wildland fire, we followed a common procedure of classifying the ventilation index into categories of poor, marginal, fair, and good. We assigned a classification scheme that is half of commonly used classes (Hardy and others 2002), however, because wind speeds at 10 m agl typically are about half of those at 40 m agl, which is closer to the height of a trajectory wind. The resulting classification scheme is summarized in Table 4.1.

Figure 4.1 illustrates the monthly mean classifications of ventilation index for May in the 48 contiguous states. Note the vast areas of relatively poor ventilation potential in the morning except in regions of high terrain. During the afternoon, the ventilation potential improves dramatically. Marginal conditions prevail, however, in the southeastern United States and in the west coastal and Appalachians mountains. The best ventilation potential during afternoons in May appears to be around and in the lee of the Rocky mountains. Monthly mean maps of the ventilation index classes are available on the VCIS web site [www.fs.fed.us/pnw/fera/vent](http://www.fs.fed.us/pnw/fera/vent) for all months and all 50 states. The interactive web site allows users to plot sensitive receptors, such as hospitals, schools, airports, wilderness areas, and highways as overlays on the ventilation index maps. In addition, users can zoom, pan, add elevation contours, cities, state and county boundaries, and rivers and railroads to help exactly locate areas or potentially high risk.



**Figure 4.1.** Monthly mean maps of ventilation index classifications for a) morning and b) afternoon in May. Red represents potentially poor ventilation conditions, yellow is marginal, green is fair, and gray is good.

In addition to maps of ventilation index classifications, the temporal variability of ventilation indexes can be viewed from the VCIS web site for any point on the landscape through frequency plots of all twice-daily values. The frequencies are shown as box plots, making it possible for users to determine the chance of experiencing a desired ventilation index value on any day of the month. Also available are plots that show the year-to-year variability of values for each month. In these plots, the index is not limited to classes but the full range of actual values can be viewed. Appendix 2 provides examples and explains how to interpret the box-plot time series of ventilation index.

## 4.1 Ventilation Index Verification

As an index, one only can judge its value from its measured components, which are wind and mixing height. Modeled winds were shown to be reasonably accurate in many cases, with randomly distributed errors within a range of observation accuracy, but there seems to be a relatively consistent slow bias, mainly during spring and early summer and in high desert regions and flat, grassy areas. Mixing heights appear reasonably accurate in all cases, except within tens of kilometers from Omaha, Nebraska and Corpus Christi, Texas. It is difficult to determine the accuracy of the local inversion potential, however, because there are so few observations. Also, the relatively coarse grid size (2.5° latitude-longitude and 5 km) does not capture many of the small hollows that can trap smoke at night. Together with the somewhat slow wind speed and inclusion of local valley inversions, we assume that the ventilation index errs conservatively, biasing toward potentially poor ventilation. While there are missing data in the 40-year record, the long time series ensures reliable interpretation of temporal patterns.

## 4.2 Key Elements of Ventilation Index

- The ventilation index derived for VCIS is most useful for addressing concerns about smoke that stays relatively close to the ground.
- The ventilation index climate is somewhat conservative but provides a reasonably accurate view of ventilation potential during the last 40 years.
- The ventilation climate information system (VCIS) provides the first national coverage of ventilation climate.

## 5.0 RISK TO AIR QUALITY AND VISIBILITY FROM WILDLAND FIRES

Development of a fine-resolution database of surface winds, mixing height, and ventilation index affords a unique opportunity to assess the risks to air quality and visibility from wildland biomass burning at a variety of scales. While model-generated data only can approximate actual conditions, the mapped products and point statistics show reasonable patterns of information and provide the most accurate representation of historical ventilation potential to date. Therefore, conclusions should be used cautiously but not without some confidence.

Risks to air quality occur when ventilation index values are low and harmful pollutants are held close to the ground. Risks to visibility also occur when ventilation index values are low. Light-scattering and absorbing elements of smoke near the ground cause significant degradation of visual range, especially when combined with high atmospheric humidity.

While we base our estimate of risks to air quality and visibility solely on an index of ventilation potential, more precise estimates can be derived by combining ventilation potential with historical smoke emissions and atmospheric humidity data. Because emissions and humidity data currently are unavailable at a consistent temporal and spatial resolution and they are much more difficult to derive

than mixing height and wind, they are not included in this assessment. Where available locally, however, they can be used to help refine the risks identified by ventilation index.

Spatial patterns of the monthly mean ventilation index can be viewed on the VCIS web site [www.fs.fed.us/pnw/fera/vent](http://www.fs.fed.us/pnw/fera/vent). In general, ventilation index data show the greatest risks to air quality and visibility in the southeastern United States, where marginal to fair ventilation conditions prevail most of the year. This region also has a high concentration of roads, hospitals, and schools. Additionally, the northern plains and deep valleys of the western United States show risk potential with consistently poor to marginal ventilation during the winter and marginal to fair conditions during spring and autumn. Sensitive receptors in the northern plains and western valleys, however, are much more sparse than in the southeastern United States.

Site-specific information on temporal patterns of ventilation indexes can be viewed from the VCIS web site by selected the “get stats” button in the maps and graphs section. At each point, periods of good ventilation potential can be found at times throughout the year. Some places have greater frequency of good ventilation and there are some times that are better than others. There also are places and times when poor ventilation conditions prevail.

To help summarize the data, we divided the country into significant airsheds as defined by the United States Geological Survey hydrologic unit code (HUC) system (Seaber et al. 1987) (Figure 5.1). The contiguous states were divided according to 1st order hydrologic units. The second-order hydrologic units were used to represent airsheds in Alaska. Hawaii is considered a single, separate airshed.

The average ventilation index for each regional airshed is shown in Table 5.1. The table is color coded to highlight values that fall into the range of index classifications of poor ( $0-1175 \text{ m}^2/\text{s}$ ), marginal ( $1176-2350 \text{ m}^2/\text{s}$ ), fair ( $2351-3525 \text{ m}^2/\text{s}$ ), and good ( $>3525 \text{ m}^2/\text{s}$ ) as red, yellow, green, and white, respectively. During morning hours, most of the country, except Hawaii, experiences relatively low ventilation potential most of the year. During winter, however, somewhat better ventilation conditions prevail during the morning in places that encounter consistently strong winds, such as where ocean and lake breezes are enhanced during winter (Mid-Atlantic, New England, Pacific Northwest, Great Lakes regions, and the southern Alaska airsheds), and leeward of the Rocky Mountains (Missouri HUC) where



Figure 5.1. Regional airshed boundaries for Alaska and the contiguous states.

downslope winds are common in winter.

Morning ventilation potential is dominated by wind, while afternoon potential is dominated by mixing height. Good ventilation potential prevails during spring and early summer in the high desert regions of the country where intense heating causes very high mixing heights. These places include the Rio Grande, Upper and Lower Colorado, and Great Basin airsheds, with good conditions extending well into early autumn in the Rio Grande airshed. The Arkansas-White-Red airshed in the south-central states also experiences good ventilation during midsummer when afternoon heating is greatest.

Counter to most of the rest of the country, the highest ventilation indexes in the Pacific Northwest occur during winter. While the Columbia Basin that is centered in the Pacific Northwest region consistently experiences marginal ventilation potential during winter, high mountains that dominate the remainder of the airshed receive their highest winds in winter, and thus high ventilation potential. Also, high terrain in the Pacific Northwest often rises above interpolated mixing height values in winter, causing the 4000 m agl arbitrary level to dominate mixing height values at this time of year. This may create artificially high ventilation potential in this airshed during winter.

**Table 5.1.** Average ventilation index values for each regional airshed and each month. Red = poor (<1175), yellow = marginal (1176-2350), green = fair (2351-3525), and white = good (>3525).

Hour	Region	January	February	March	April	May	June	July	August	September	October	November	December
AM	Arkansas-White-Red	1698.665	1882.891	2152.282	2042.367	1915.744	1566.713	1341.4821	1247.8405	1510.088	1652.478	1904.084	1800.218
	California	2333.697	2388.604	2313.159	2125.415	2040.363	1757.431	1525.5821	1396.0055	1638.881	1792.618	2176.026	2265.437
	Great Basin	1825.842	1927.09	2037.642	1882.237	1677.479	1397.735	1352.9542	1282.1343	1448.515	1513.094	1862.428	1881.357
	Great Lakes	3713.367	3095.291	3362.655	3272.749	2371.36	2048.857	1615.9821	1809.3184	2380.839	3325.296	4134.547	3959.198
	Lower Colorado	2128.778	2088.893	2231.951	2087.177	1826.8	1573.981	1466.0403	1419.0378	1695.642	1851.805	2002.384	2065.047
	Lower Mississippi	1577.653	1794.816	1895.963	1660.973	1541.267	1100.7	862.6705	794.5333	1121.718	1252.175	1787.054	1761.545
	Mid-Atlantic	2911.525	2753.685	2849.109	2700.86	2099.958	1796.274	1586.9967	1612.3972	1775.999	2223.171	2775.081	2798.968
	Missouri	2421.245	2187.915	2343.449	2321.626	2031.493	1678.611	1386.4606	1396.9675	1805.89	2183.554	2318.715	2335.957
	New England	2965.384	2783.926	3163.591	3032.842	2396.205	2150.603	1834.3067	1883.0277	2092.406	2552.605	3214.579	2953.982
	Ohio	2751.563	2385.582	2536.225	2521.763	1808.839	1412.978	1190.4821	1175.2388	1450.866	1836.437	2505.168	2635.558
	Pacific Northwest	2818.258	2725.941	2495.324	2249.026	1978.593	1808.548	1637.895	1569.1146	1838.681	2181.133	2770.237	2769.294
	Rio Grande	1887.143	1928.383	2173.831	2004.244	1840.387	1548.882	1319.0639	1252.0107	1482.335	1647.288	1922.719	1862.716
	Souris-Red-Rainy	1925.715	1815.38	2130.108	1940.212	1803.527	1616.724	1198.5647	1340.6457	1892.266	2483.151	2228.174	1889.945
	South Atlantic-Gulf	1525.217	1741.52	1748.835	1576.024	1335.604	1215.232	1114.6528	1069.8131	1210.323	1244.047	1492.517	1505.974
	Tennessee	2178.679	2206.844	2256.474	2169.307	1769.48	1371.949	1212.13	1159.8289	1410.031	1694.721	2158.289	2232
	Texas-Gulf	1415.034	1666.869	1889.345	1924.54	2061.892	1814.636	1483.5088	1334.6003	1374.987	1441.274	1684.803	1583.626
	Upper Colorado	1970.786	1896.997	2213.956	2052.606	1835.84	1568.237	1406.5466	1388.0983	1653.867	1743.939	2043.929	2009.954
	Upper Mississippi	2002.925	1773.155	2215.923	2109.35	1668.66	1390.749	1057.6634	1098.6601	1462.063	1958.81	2129.315	2008.034
	PM	Arkansas-White-Red	3238.164	3890.885	5295.21	6705.227	6426.541	6671.674	8339.209	7626.044	6363.746	4650.421	3951.178
California		5822.603	5144.75	4999.277	5456.225	5664.775	5997.945	5991.108	5674.538	5019.343	4531.166	5337.295	6009.391
Great Basin		4454.25	4092.097	5414.504	6412.604	6763.791	7794.634	7767.917	7020.71	5985.367	4352.38	4202.549	4402.25
Great Lakes		3750.201	3802.654	4823.678	6631.787	6504.262	6430.412	5876.322	5523.516	5462.561	5117.806	4293.968	3617.901
Lower Colorado		3619.855	4019.788	6099.871	7863.151	8746.685	9884.428	8255.318	6813.053	6346.735	4870.073	3982.033	3473.95
Lower Mississippi		2930.096	3526.086	4515.544	5159.906	4952.011	4906.873	4815.451	4725.205	4661.221	3898.253	3558.338	2973.252
Mid-Atlantic		4199.54	4218.405	4796.287	5523.364	5274.652	5178.488	4805.478	4337.859	4063.727	4070.122	4143.97	4331.952
Missouri		4770.698	4288.022	5005.896	6964.083	6573.279	6497.427	6609.299	6212.683	5497.959	4921.312	4587.563	4649.465
New England		4793.601	4798.913	5367.692	5752.979	5569.468	5610.639	5019.91	4635.578	4426.525	4526.721	5038.46	4594.267
Ohio		3317.016	3345.305	4520.339	5528.495	5182.007	4894.639	4508.169	4298.267	4400.441	3938.195	3634.8	3249.166
Pacific Northwest		8714.619	6438.289	5009.993	5236.998	5231.132	5617.919	6041.011	5694.01	4651.215	4451.232	6980.375	8755.976
Rio Grande		4217.177	5352	7847.93	9429.945	10673.133	11131.527	9794.511	7755.476	7120.881	5629.02	4645.472	4293.127
Souris-Red-Rainy		2485.233	2751.729	3575.949	6243.549	6585.363	6100.571	5498.189	5257.993	4837.219	4275.988	2861.141	2189.06
South Atlantic-Gulf		2973.66	3624.151	4511.679	5154.71	4944.432	4735.611	4675.203	4210.113	4086.641	3681.942	3298.799	2943.751
Tennessee		3790.845	3981.517	4778.239	5488.574	4961.649	4734.567	4414.173	4122.66	4213.317	3849.989	3831.033	3912.683
Texas-Gulf		2969.144	3585.965	4863.129	5873.144	5899.422	5768.874	6969.451	6971.293	5483.046	4291.183	3688.705	2958.892
Upper Colorado		5863.141	4808.765	5626.229	6809.718	7336.497	7860.853	6918.882	6218.836	5837.513	4374.608	4925.776	5749.428
Upper Mississippi		2425.755	2500.116	3816.998	5562.746	5613.912	5170.826	4540.032	4234.709	4238.462	3806.288	2910.214	2300.078

While prevailing ventilation conditions may indicate the likelihood of risk to values of air quality and visibility in each region, in all places at many times of the year, good ventilation conditions can occur. The "Get Stats" button from the Maps and Graphs page of the ventilation index climate system web site <http://www.fs.fed.us/pnw/fera/vent> shows the frequency of potentially good ventilation potential on any day of the month or any month of the year for individual grid points. To illustrate the regional variability of the ventilation index, we created a series of box plots that show the median standard deviation and range of values for each month. While the ventilation index ranges from zero to well over 70,000 m<sup>2</sup>/s, the box plots are truncated at 14,000 m<sup>2</sup>/s in the afternoon and 7,000 m<sup>2</sup>/s in the morning to

better illustrate the range of management categories, where any value above 3,525 m<sup>2</sup>/s is considered good ventilation potential.

From the box plots (see Appendix 3) it appears that all areas can experience good ventilation and low risk to values of air quality and visibility at times during the morning (range bars exceed 7000 m<sup>2</sup>/s) but the Great Lakes region clearly experiences the best morning ventilation potential within a standard deviation of its median, especially during winter. The standard deviations of values generally range from poor to fair during the morning in most regions. This suggests almost nationwide, values of air quality and visibility are most likely to be affected during the late night and early morning.

The box plots show that most places have significant potential (within a standard deviation of their median) of reaching good ventilation conditions during the afternoon at any time of the year. Exceptions include the Upper and Lower Mississippi regions, which while exhibiting some good ventilation occurrences at all times of the year, struggle to reach fair conditions in winter and good conditions occur within a standard deviation only in April and May. This suggests that it may be more difficult to find good ventilation conditions in the Mississippi regions than in others.

Another note of interest is the large range of ventilation conditions in California. Its box plot shows that the frequency of good conditions is nearly the same as the frequency of very poor conditions, no matter what time of year. While other regions may confidently expect good ventilation conditions in July, for example, the chances of finding good conditions in the California region are equal to finding poor conditions. This makes seasonal planning in the California region more difficult than for other regions.

The data suggest that all areas experience times of good ventilation. Therefore, it should be possible to mitigate potential impacts on values of air quality and visibility. In some places, however, good ventilation conditions are less frequent than marginal or poor ventilation conditions and during the morning good ventilation is infrequent in most places. At these times and places, managing against the risk to air quality and visibility may be challenging. The data show highly variable conditions, however, in both space and time. The Ventilation Climate Information System, which illustrates the frequency and spatial distribution of ventilation conditions that may impact values of air quality and visibility, should quantify potential risks.

## **5.2 Key Elements of Risks to Air Quality and Visibility from Wildland Fire**

- Risks to air quality and visibility from wildland fire can be estimated by assessing spatial and temporal patterns of ventilation index.
- The greatest risks to air quality and visibility from wildland fire occur in the southeastern United States.
- Risks to air quality and visibility from wildland prescribed fire can be minimized by planning times when good ventilation conditions are most frequent.
- The best ventilation conditions during morning hours occur during winter along the northern coasts of the 48 states, southern Alaska, and in the north-central plains.
- The best ventilation conditions during afternoon hours occur in spring and early summer in Rio Grande airshed.

- The VCIS point statistics allow identification of times of highest or lowest risk at any point on the landscape.
- The VCIS monthly maps show places the spatial patterns of potential risk.

## 6.0 CONCLUSIONS

The Ventilation Climate Information System allows for assessing values of air quality and visibility at risk from wildland fire by illustrating the spatial and temporal variability of ventilation potential. The 40-year, twice-daily time series at 2.5' latitude-longitude and 5-km spatial resolution can be viewed as monthly averaged maps of index classifications or in plots of frequency and magnitude at selected points. The ArcIMS web-access system allows users to view local to national patterns of ventilation potential. Overlays of sensitive receptors (hospitals, schools, roads, airports, etc.) can help quantify the proximity of risk to poor ventilation conditions.

Creation of such a high-resolution climate information system, with over 100 GigaBytes of data, was only possible with today's computing power. Even so, the amount of smoothing and simplifying assumptions needed to process the data in a reasonable amount of time could be reduced with even more computational energy. Also, while the long record may compensate for missing data, increased computer resources could reduce the number of missing values. Nevertheless, the generated values provide a reasonably accurate view of ventilation potential and associated risks to air quality and visibility in the United States. The products include several unique features:

- The first nationally consistent, historical database of surface wind at fine spatial resolution.
- The longest historical record and finest spatial resolution of mixing height.
- The first database of historical ventilation potential.
- The first physically reasonable assessment of historical risks to air quality and visibility.

Because the VCIS offers the first historical perspective of ventilation potential and associated risks to air quality and visibility at a high spatial and temporal resolution on a national scale, the information it holds about patterns and probabilities of risk are just beginning to be explored. As users are being introduced to the products, however, several applications to land management emerge. These include:

- Identification of areas at risk to smoke problems
- Smoke Management Planning
- Airshed assessments
- Better understanding of the spatial and temporal variability of atmospheric conditions that affect smoke dispersion.

While we adopted a relatively simple approach to assessing values at risk, it was not a trivial task to create the necessary products for analysis. As use increases, however, it may become beneficial to add detail and increase accuracy. For example, the 2.5' latitude-longitude and 5 km spatial resolutions are considered extremely fine for such a long history and large domain. Land managers, however, work at

resolutions closer to 1 km or less and may desire information more than twice a day. With greater resources it is possible to downscale each product and add accuracy. Until then, we hope users of this first rendition of the Ventilation Climate Information System will find value in the information and tools offered from the Internet map server.

## 7.0 LITERATURE CITATIONS

**Achtemeier, G.L., W. Jackson, B. Hawkins, D.D. Wade, and C. McMahon. 1998.** The smoke dilemma: a head-on collision! Transactions of the 63<sup>rd</sup> North American Wildlife and Natural Resource Conference. 20-24 March 1998. Orlando FL. 415-421.

**Alpert, P.; Getenio, B.; Zak-Rosenthal, R. 1988.** One-level modeling for diagnosing surface winds over complex terrain: II. applicability to short-range forecasting. Monthly Water Review. 116(10): 2407-2461.

**Alpert, P.; Getenio, B. 1988.** One-level diagnostic modeling of mesoscale surface winds in complex terrain: I. comparison with three-dimensional modeling in Israel. Monthly Weather Review. 116(10): 2025-2046.

**Alpert, P. 1988.** The combined use of three different approaches to obtain the best estimate of meso-surface winds over complex terrain. Boundary-Layer Meteorology. 45: 291-305.

**Cressman, G.P. 1959.** An operational objective analysis system. Monthly Weather Review. 87: 367-374.

**Danard, M. 1977.** A simple model for mesoscale effects of topography on surface winds. Monthly Weather Review. 105: 572-580.

**Dempsey, D.P. 1985.** A one-level mesoscale model for diagnosing surface winds in mountainous and coastal regions. University of Washington. Ph.D. dissertation.

**Grell, G.A., J.Dudhia, and D.R. Stauffer. 1994.** A description of the fifth-generation Penn State/NCAR Mesoscale Model (MM5). NCAR Technical Note, NCAR/TN-398 + STR. Mesoscale and Microscale Meteorology Division, National Center for Atmospheric Research, Boulder, Colorado. 121 pp.

**Hardy, C.; Ottmar, R.D.; Peterson, J.; Core, J. 2002.** Smoke management guide for prescribed and wildland fire—2000 edition. Boise, ID: National Wildfire Coordinating Group. [in press].

**Holzworth, G.C. 1972.** Mixing heights, wind speeds, and potential for urban air pollution throughout the contiguous United States. Office of Air Publication No. AP-101. Research Triangle Park, NC: United States Environmental Protection Agency, Office of Air Programs.

**Holzworth, G.C.; Fisher, R.W. 1979.** Climatological summaries of the lower few kilometers of

rawinsonde observations. United States Environmental Protection Agency, Office of Research and Development, Research Triangle Park, North Carolina. 140 pp.

**Kalnay, E.; Kanamitsu, M.; Kistler, R.; Collins, W.; Deaven, D.; Gandin, L.; Iredell, M.; Saha, S.; White, G.; Woollen, J.; Zhu, Y.; Chelliah, M.; Ebisuzaki, W.; Higgins, W.; Janowiak, J.; Mo, K.C.; Ropelewski, C.; Wang, J.; Leetmaa, A.; Reyholds, R.; Jenne, R.; Joseph, D. 1996.** The NCEP/NCAR 40-year reanalysis project. *Bulletin of the American Meteorological Society*. 77(3): 437-471.

**Lipsett M., Hurley S., Ostro B. 1997.** Air Pollution and Emergency Room Visits for Asthma in Santa Clara County, California. *Environmental Health Perspectives*. 105(2):216-222.

**Manning, K.W.; Haagenson, P.L. 1992.** Data ingest and objective analysis for the PSU/NCAR modeling system: Programs DATAGRID and RAWINS. NCAR Technical Note NCAR/TN-376+IA. [Boulder, CO]: [National Center for Climate Research]. 209 pages.

**Mass, Clifford F.; Dempsey, David P. 1985.** A one-level, mesoscale model for diagnosing surface winds in mountainous and coastal regions. *Monthly Weather Review*. 113:1211-1227.

**National Climatic Data Center. 1997.** Hourly United States weather observations 1990-1995. National Climatic Data Center, 151 Patton Avenue, Asheville, NC 28801 and United States Environmental Protection Agency, Research Triangle Park, Raleigh, NC.

**National Renewable Laboratory. 1992.** National solar radiation data base 1961-1990. Volume I, II, and III. National Climatic Data Center, Federal Building, Asheville, NC, 28801.

**Neff, W.D.; King, C.W. 1989.** The accumulation and pooling of drainage flows in a large basin. *Journal of Applied Meteorology*. 28: 518-529.

**Pasquill, F. 1962.** Atmospheric diffusion. London: Van Nostrand. 209.

**Ruthford, J; Ferguson, S. 2001.**

**Schwartz J, Slater D, Larson T.V, Pierson W.E, Koenig J.Q. 1993.** Particulate air pollution and hospital emergency room visits for asthma in Seattle. *Am Rev Respir Dis*. 147(4):826-831.

**Seaber, P.R; Kapinos, F.P.; Knapp, G.L. 1987.** Hydrologic units maps. Water Supply Paper 2294. United States Geological Survey. 63 pp.

**South Carolina Forestry Commission. 1996.** Smoke Management Guidelines for Vegetative Debris Burning Operations: State of South Carolina. SCFC 3<sup>rd</sup> Printing. 19 pp.

**Speers P.; Mass, C.F. 1986.** Diagnosis and prediction of precipitation in regions of complex terrain. WSDOT Final Report WA-RD-91.1. Washington State Department of Transportation, Transportation Building, Olympia, WA 98504. 166 pp.

**Turner, D. B., 1964.** A dispersion model for an urban area. *Journal of Applied Meteorology*. 3: 83-91.

**United States Department of the Interior. 1995.** Remote Automated Weather Stations (RAWS) and

Remote Environmental Monitoring Systems (REMS) Standards for the United States Department of the Interior, Bureau of Land Management. Boise, ID: Bureau of Land Management; National Fire Information Center.

**USDA Forest Service, Southern Forest Experiment Station.** 1976. Southern forestry smoke management guidebook. United States Department of Agriculture, Forest Service, Southern Forest Experiment Station. SE-10. 55 pp.

**United States Environmental Protection Agency.** 2001. Office of Air Quality Planning and Standards (OAQPS) Technology Transfer Network (TTN), Support Center for Regulatory Air Models (SCRAM). [www.epa.gov/scram001].

**United States Environmental Protection Agency.** 1997. National Ambient Air Quality Standards for Particulate Matter; Final Rule. 40 CFR Part 50 [AD-FRL-5725-2] RIN 2060-AE66. Federal Register. 62(138): 102 pp.

**Utah Administrative Code.** 2001. Emission standards: General Burning. R307-202. Michael G. Broschinsky, Administrative Code Editor, Division of Administrative Rules, PO Box 141007, Salt Lake City, Utah 84114-1007.

**Wade, D.D.** 1989. A Guide for prescribed fire in southern forests. National Wildfire Coordinating Group, Prescribed Fire and Fire Effects Working Team, Boise Interagency Fire Center, ATTN: Supply, 3905 Vista Avenue, Boise, ID 83705. NFES #2108. [United States Department of Agriculture, Forest Service, Southeastern Forest Experiment Station. Tech. Pub. R8-TP 11.] 56 pp.

## APPENDIX 1: Map Projections

**Data Projections:** To generate the spatial data components of wind, mixing height, and ventilation index, we used geographic coordinates for the contiguous 48 states and Hawaii, with a grid resolution of 2.5-minute latitude/longitude. The geographic coordinate system creates excessively elongated grid cells above the 50th parallel, however, which cause computational problems for the wind model. Therefore, in Alaska an Albers Conical Equal Area projection was used for generating spatial components, with a grid resolution of 5 km. The following is a summary of map projections used to generate spatial data components of wind, mixing height, and ventilation index:

### Contiguous 48 States and Hawaii:

- Projection: Geographic
- Units: Decimal degrees
- Spheroid: WGS84
- Grid size: 2.5 minutes

### Alaska:

- Projection: Albers Conical Equal Area
- First standard parallel: 58 00 00
- Second standard parallel: 68 00 00
- Central meridian: -150 00 00
- Origin of the projection: 50 00 00
- False easting: 0
- False northing: 0
- Spheroid: North American Datum 1983
- Grid size: 5000 meters

**Web Map Projections:** To generate monthly mean maps of the spatial data for display on the web, we used projections that are common to each region to create maps that look familiar to most users. The following is a summary of map projections used to generate web maps:

### Contiguous 48 States:

- Projection: Albers Conical Equal Area
- First standard parallel: 29 30 00
- Second standard parallel: 45 30 00
- Central meridian: -96 00 00
- Origin of the projection: 23 00 00
- False easting: 0
- False northing: 0
- Spheroid: North American Datum 1983
- Grid size: 5000 meters for meteorological data, 2500 meters for background terrain

Alaska:

- Projection: Albers Conical Equal Area
- First standard parallel: 58 00 00
- Second standard parallel: 68 00 00
- Central meridian: -150 00 00
- Origin of the projection: 50 00 00
- False easting: 0
- False northing: 0
- Spheroid: North American Datum 1983
- Grid size: 5000 meters for meteorological data, 2500 meters for background terrain

Hawaii:

- Projection: Universal Transverse Mercator
- Zone: 4
- Spheroid: North American Datum 1983
- Grid size: 5000 meters for meteorological data, 2500 meters for background terrain

## APPENDIX 2: How to Interpret Graphics

### A2.1 How to Interpret Wind Roses

Wind roses simultaneously display wind speed, wind direction, and relative frequency.

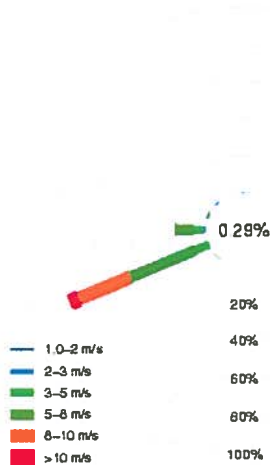
- Wind speeds are shown in units of meters per second (m/s). One m/s = 1.94 knots = 2.24 miles per hour.
- The percentage of calm winds (<1 m/s) is shown in the center of each wind rose.
- Wind speeds are represented by line thickness. Higher wind speeds are indicated by thicker lines.
- The direction that the wind comes from is represented by the angle in which a ray radiates out from the center of the plot. Straight up indicates winds coming from true north.
- Wind frequency is indicated by the length of each line segment of a given thickness and direction. The numerical labels on the concentric circles provide a scale for each graph.

#### Wind Rose Example:

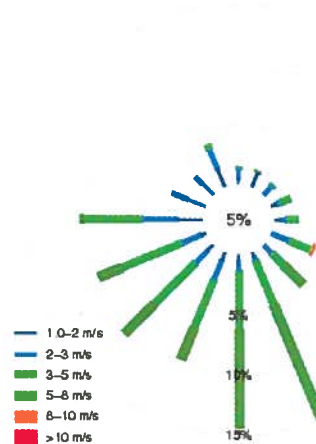
The figures below show wind frequencies from a site in California (left) and Wisconsin (right) in August in the afternoon.

- The California site indicates winds predominantly blow from the southwest at this time, and wind speeds frequently exceed 8 m/s. Only 0.29 percent of the winds are calm (less than 1 m/s).
- The Wisconsin site shows winds prevailing from the south-southeast and south at this time but a significant number of events produce southwest to west winds over the site. Few winds exceed 8 m/s and winds less than 3 m/s occur from all directions.

Wind Rose – 00Z – Aug – N 35°18.75' W 119°46.25'



Wind Rose – 00Z – Aug – N 46°36.25' W 88°33.75'



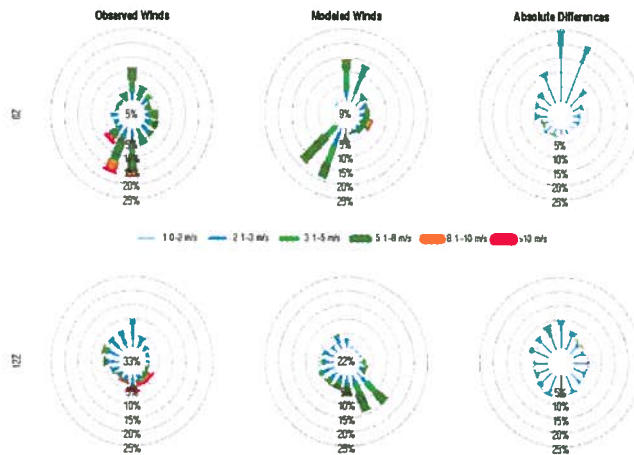
## A2.2 How to Interpret Wind Verification Plots

Polar plots of the absolute differences in winds are similar to wind roses in that they simultaneously show differences in speed, direction, and frequency.

- Absolute difference is determined by subtracting each observation from its corresponding modeled value. When observed winds are less than 1 m/s, however, they and the corresponding modeled winds are excluded from difference calculations.
- Some differences may be caused by the model itself, others may be due to the differing resolutions between the model topography and the actual topography. Measuring anemometers are sensitive to small variations in terrain and land use that are not captured in the modeling resolution. See diagrams of surrounding topography and land use that accompany each difference plot to determine this effect.
- Differences between modeled and observed wind speeds are presented as positive values, not distinguishing between overestimation and underestimation. Difference in speed is represented by line thickness, using the same speed classes as wind roses, except that differences (<1 m/s) are not a separate category; causing the thinnest line segments to represent all wind speed differences less 2 m/s.
- Difference in direction is represented by the angle in which a ray radiates out from the center of the plot. Straight up indicates essentially no difference (within 11.25 degrees). An angle of 90 degrees indicates that the modeled winds differ from the observed winds by 90 degrees in the clockwise direction (i.e., an observed direction of northeast and a modeled direction of southeast).
- Differences are calculated at standard synoptic times of 0Z and 12Z.

### Example Wind Verification:

- This figure illustrates two sites, one in each row. The top row illustrates a site for which the modeled data match the observed data reasonably well with respect to both direction and speed. This is demonstrated by the long, thin lines pointing towards the top of the absolute differences plot. The second row illustrates a site for which the modeled data do not match the observed data well, as indicated by the shorter, thicker lines pointing in all directions in the absolute differences plot.



## A2.3 How to Interpret Box Plots

Box plots simultaneously illustrate variability within and among groups of data.

- The horizontal bar indicates the median (50th percentile) of the subset.
- The lower and upper limits of the rectangle indicate the quartiles (25th and 75th percentiles, respectively) of the subset.
- The horizontal brackets at the ends of the whiskers indicate the extreme values (maximum and minimum) of the subset.
- The vertical scale of each plot is set to minimize overbearing influence of extreme upper values, and enhance detail in the majority of values. This is done by excluding 0.05% of the values that may plot above the highest thousandth tick mark of the graph.

### Mixing Height

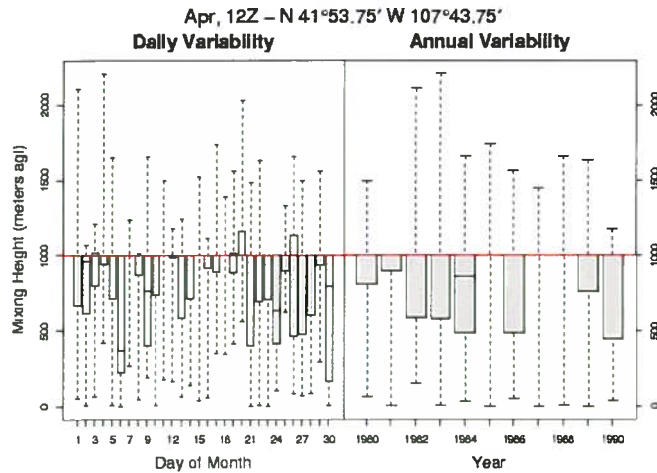
There is a horizontal line at 4000 meters on PM box plots and at 1000 meters on AM box plots.

- Interpolated mixing height values sometimes intersect high terrain, creating a belowground value. The planetary boundary layer, however, is well above ground at these places, which would allow significant ventilation to occur.
- Because positive mixing height values are needed to calculate ventilation indexes, we set a height to represent the planetary boundary layer whenever interpolated values were less than or equal to zero. The heights were arbitrarily set at 1000 meters above ground level (m a.g.l) in the morning and 4000 m a.g.l. in the afternoon, which approximate mean values of mixing heights at those times. Unfortunately, the twice-daily time series of historical mixing heights are skewed to these corrected values, especially at high elevation grid locations.
- Each box plot of mixing height includes a red, horizontal line showing the 1000 m and 4000 m level, where applicable, to help the user determine the effect of the below-ground correction.

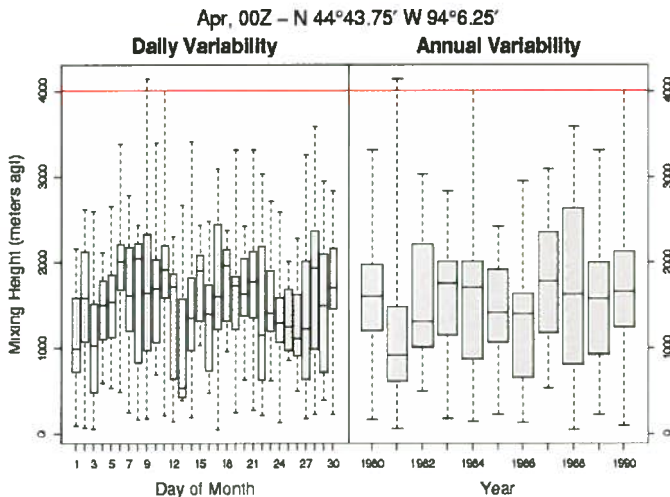
### Example Mixing Height Box Plot:

The box plots below illustrate the variability of morning mixing height for a site in Wyoming and afternoon mixing height for a site in Minnesota.

- The left side of each figure illustrates the variability within each day of the month across multiple years, whereas the right side of each figure illustrates the variability within the month from year to year.



**AM Mixing Height in April at a point in Wyoming.** The horizontal line shows the 1000 m correction for belowground mixing height values in the morning. Many times during this month at this site, mixing height is interpolated to a point below ground, and then adjusted to 1000 m. Because there are so many values at 1000 m, at times the 50th percentile and 75th percentile equal 1000 m, causing no box to appear (e.g., April 15 and 18, and 1985, 1987, and 1988).



**PM Mixing Height in April at a point in Minnesota.** The horizontal line shows the 4000 m correction for belowground mixing height values in the afternoon. At this site in this month at this time, mixing height is commonly between 1000 and 3000 meters above ground.

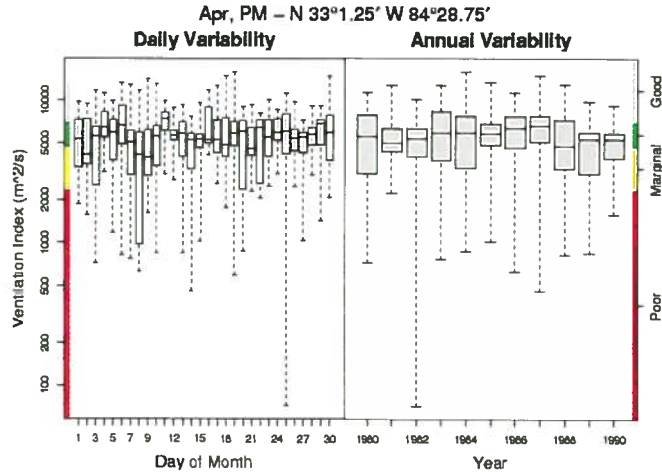
### Ventilation Index

- Ventilation Index box plots use a logarithmic vertical scale. This is to allow more visible detail.
- Color bars on each side of the ventilation index box plots show how the scale relates to mapped categories.
  - Red = poor
  - yellow = marginal
  - green = fair
  - white or gray = good

**Example Ventilation Index Box Plot:**

The box plot below illustrates the variability of morning mixing height for a site in Georgia in the afternoon.

- The left side of the figure illustrates the variability within each day of the month across multiple years, whereas the right side of each figure illustrates the variability within the month from year to year.
- Color bars on figure shows that most of the ventilation index values occur in the marginal to fair range at this site in April.



**A2.4 How to Interpret Maps**

**AM Monthly Mean Mixing Height**

Artifacts in mapped mixing height values appear at the boundaries of local occurrence neighborhoods. This is because local inversion potential is invoked only when certain conditions are met at a nearby surface observation station and adjacent surface stations may have different conditions.

**Monthly Mean Ventilation Index**

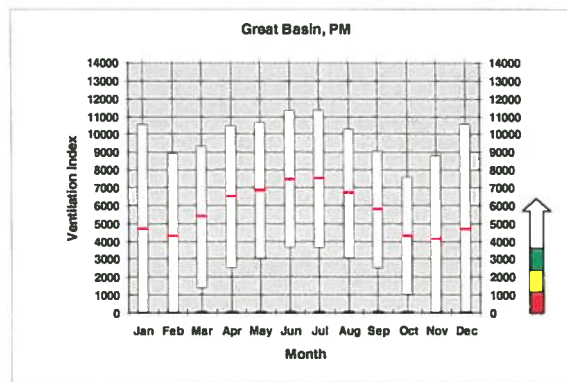
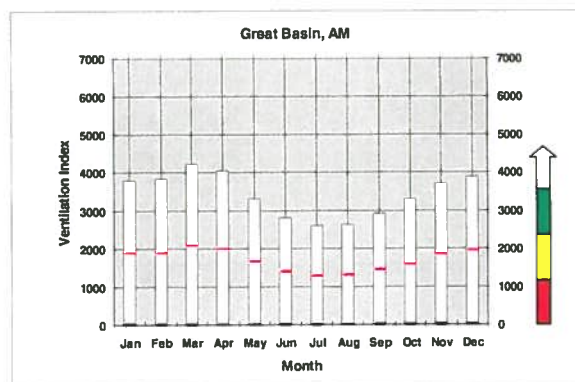
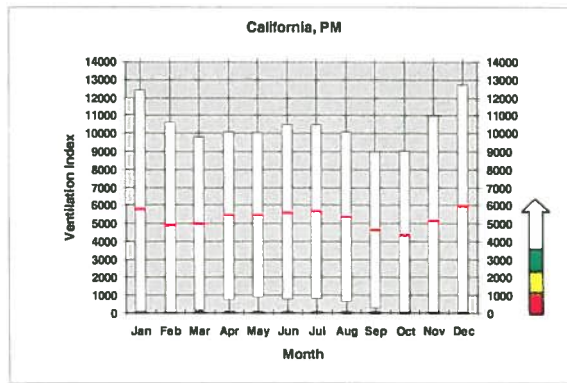
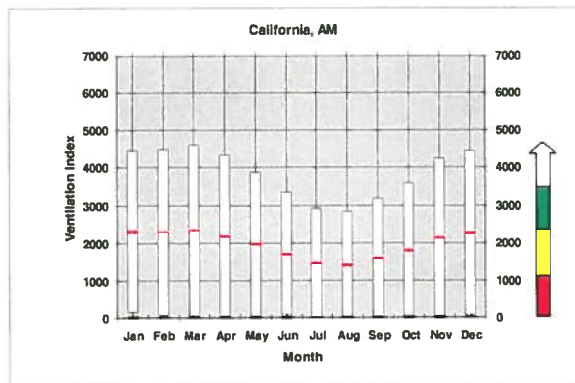
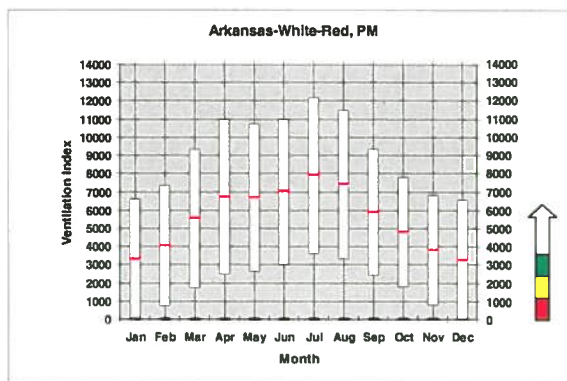
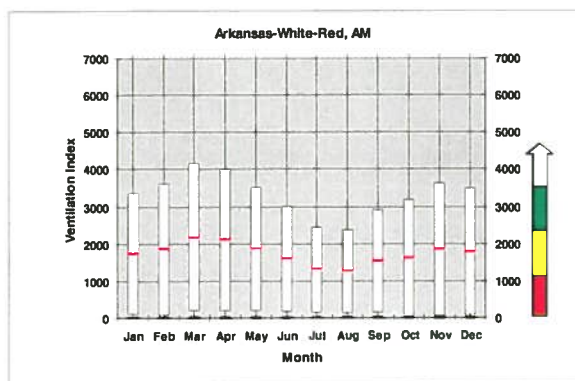
While ventilation index is calculated as a continuum of values, only four classes are plotted in the monthly mean maps. This is to facilitate the use of mapped data for assessing potential risk to values of air quality and visibility from wildland fire. The color scale is half the value of common classification schemes used by smoke managers (Hardy et al 2002). This is because wind speeds at 10 m agl typically are half of speeds at 40 m agl, a typical height of trajectory winds.

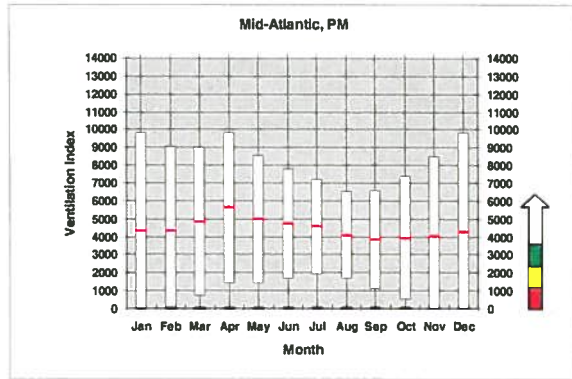
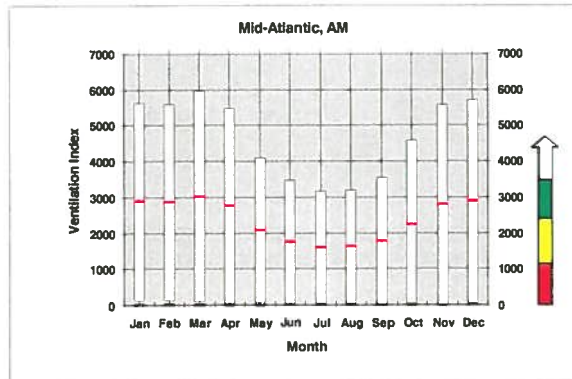
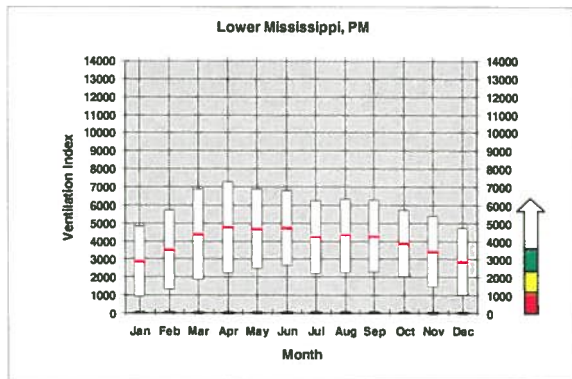
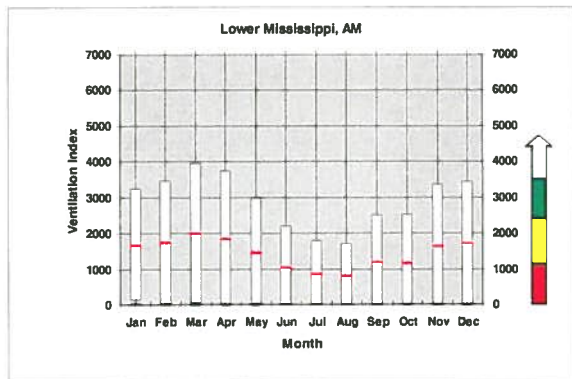
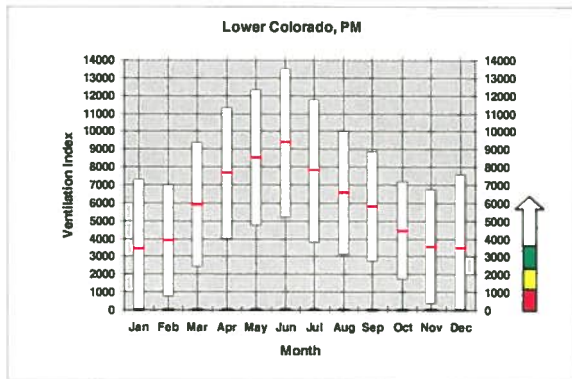
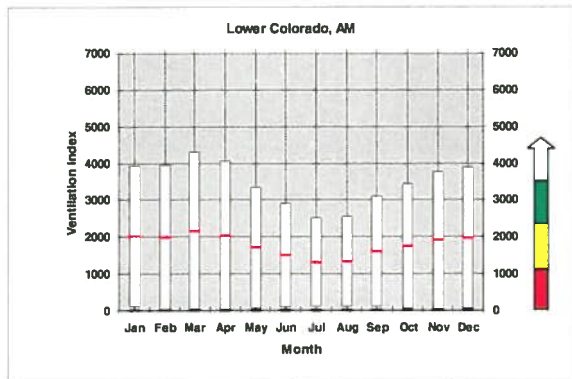
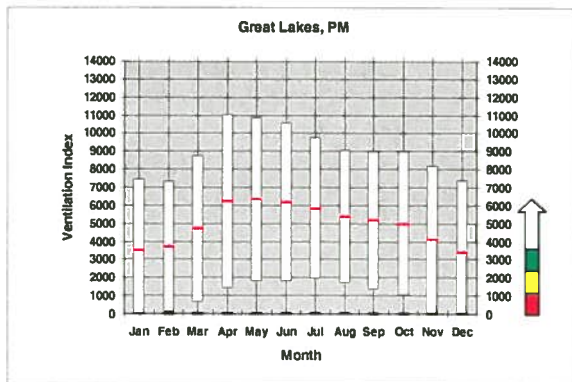
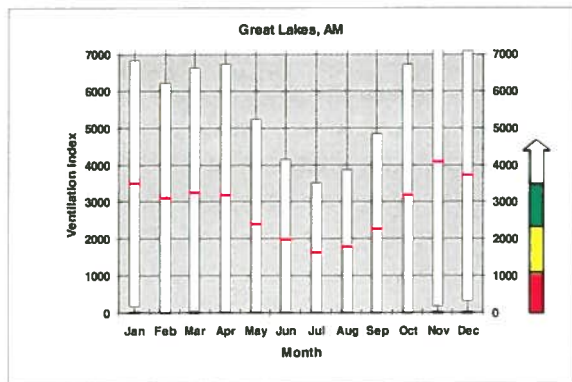
Ventilation Index (m/s)	Classification
0-1175	Poor
1176-2350	Marginal
2351-3525	Fair
> 3525	Good

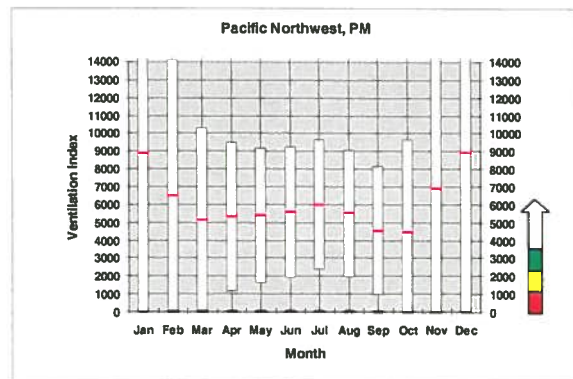
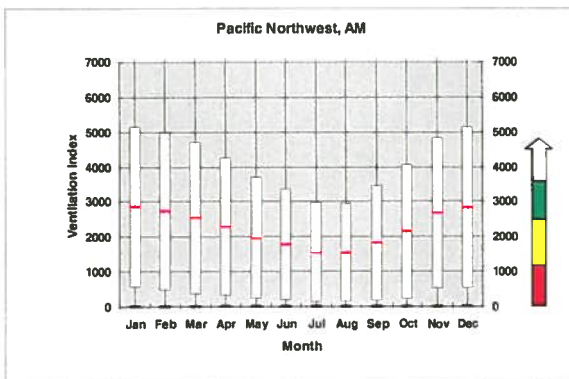
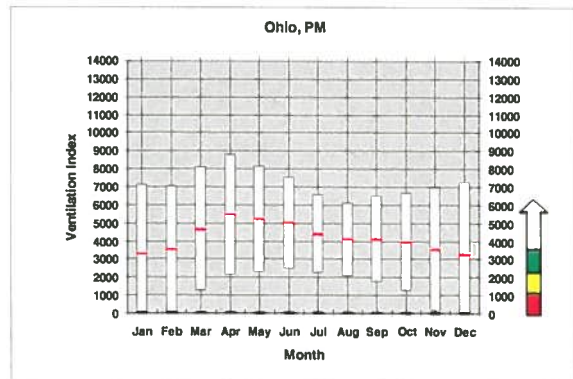
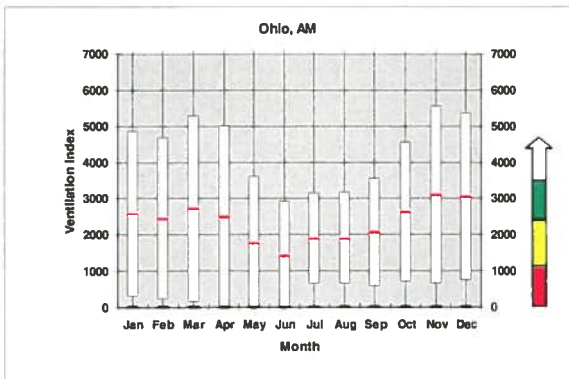
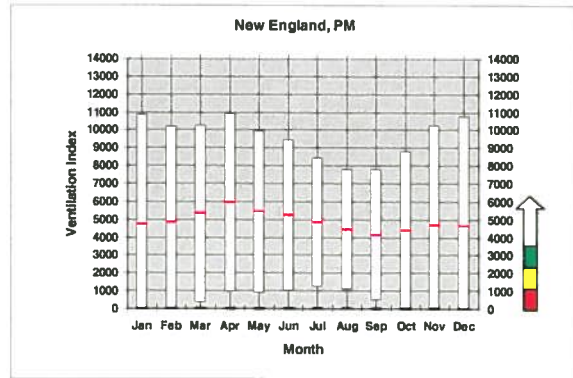
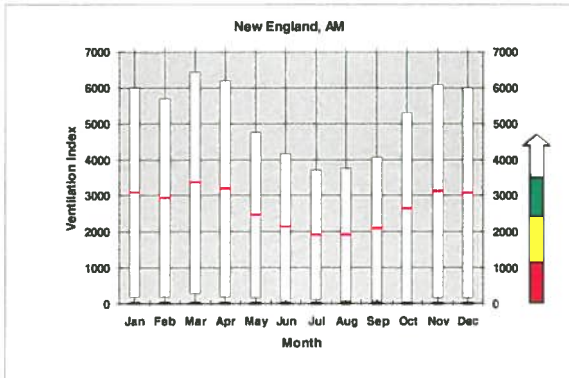
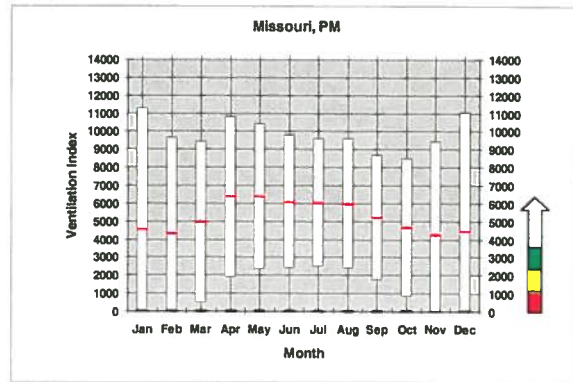
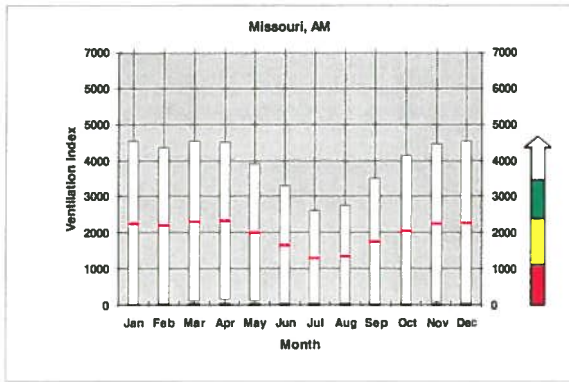
## APPENDIX 3: Summaries of Ventilation Index by Regional Airshed

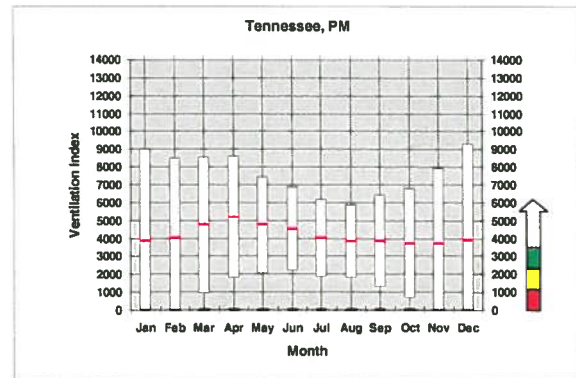
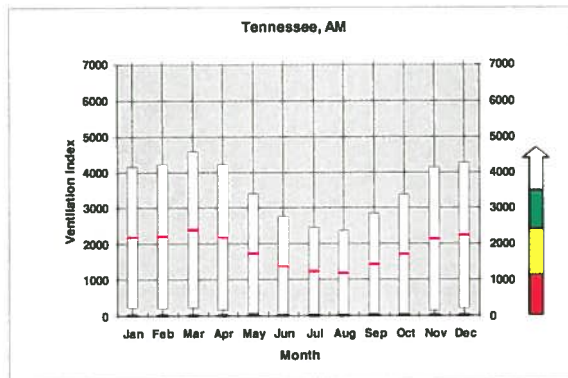
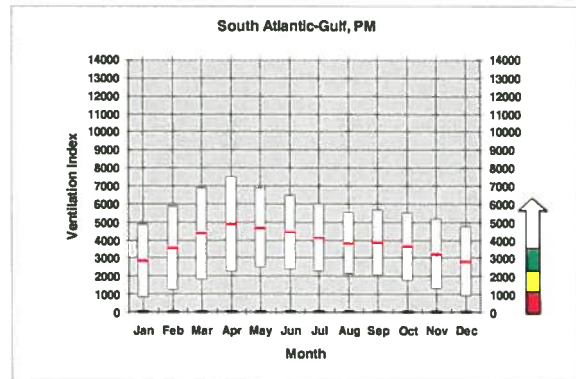
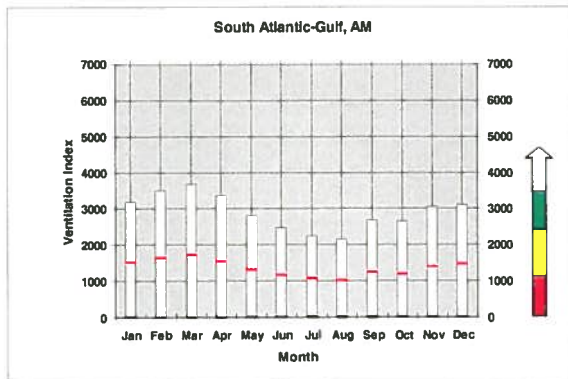
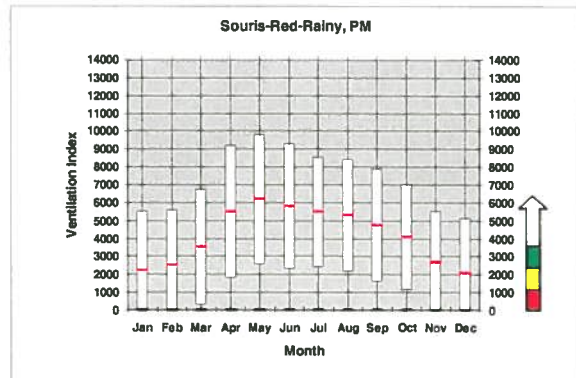
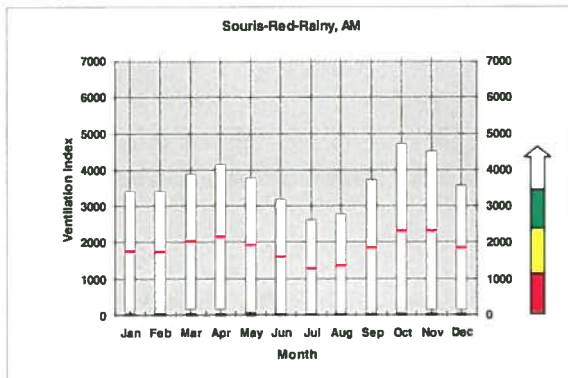
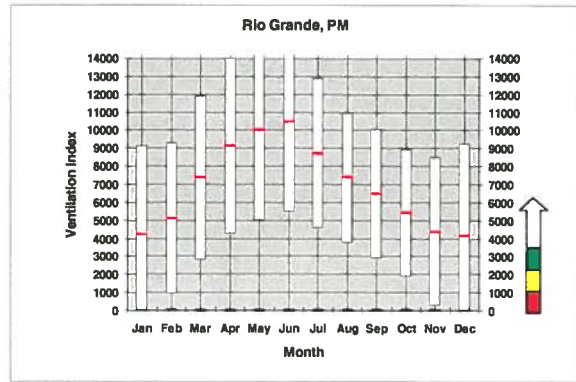
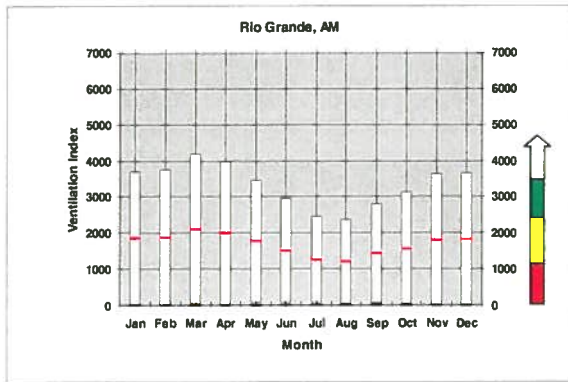
Box plots show the median standard deviation and range of values for each month in each regional airshed. While the ventilation index ranges from zero to well over 70,000 m<sup>2</sup>/s, the box plots are truncated at 14,000 m<sup>2</sup>/s in the afternoon and 7,000 m<sup>2</sup>/s in the morning to better illustrate the range of management categories, where any value above 3,525 m<sup>2</sup>/s is considered good ventilation potential. Airsheds are defined by HUC code (Seaber et al. 1987) (Figure 5.1). The contiguous states were divided according to 1st order HUC. Second-order HUCs were used to represent airsheds in Alaska. Hawaii is considered a single, separate airshed.

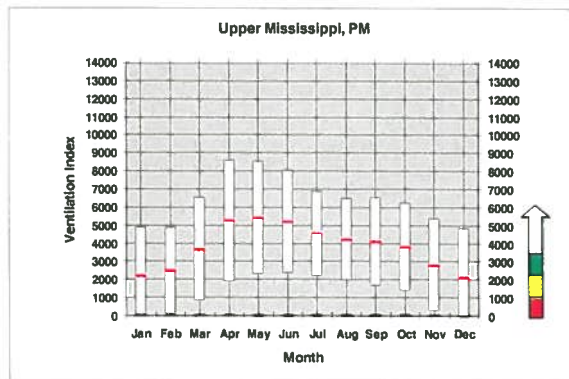
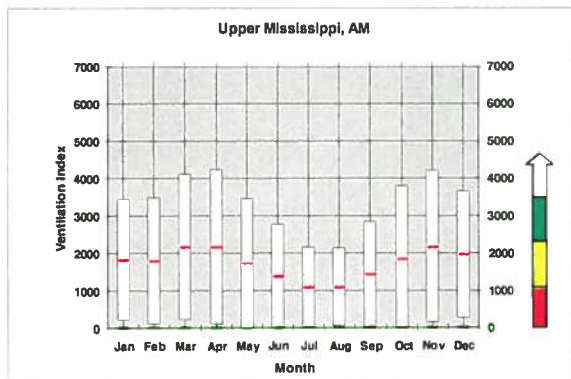
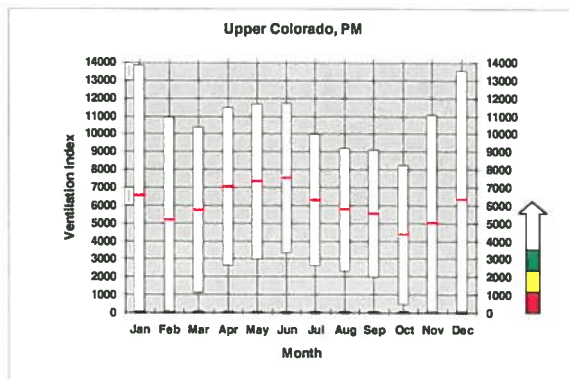
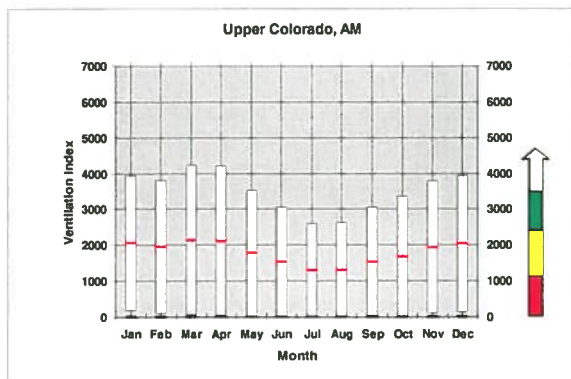
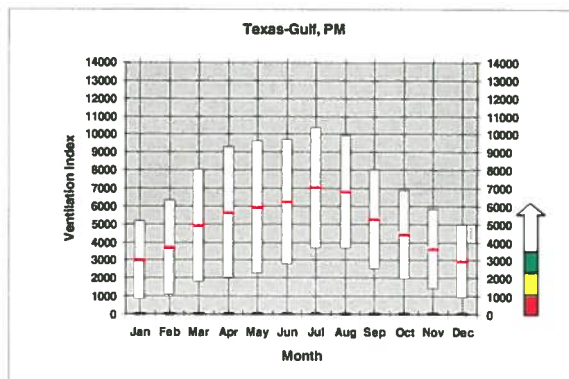
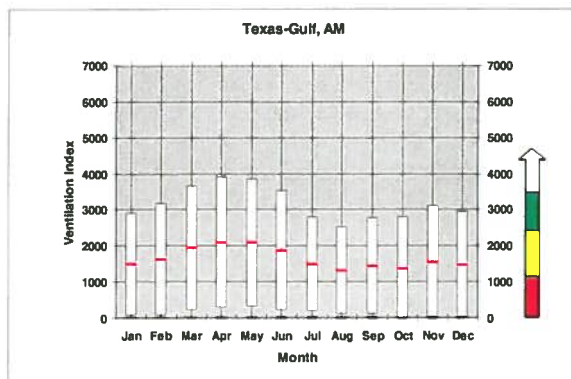
### A3.1 The 48 Contiguous States



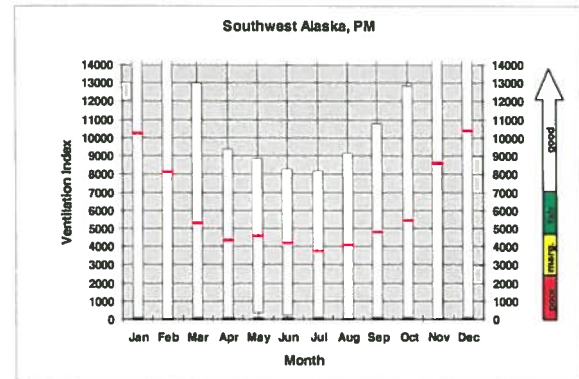
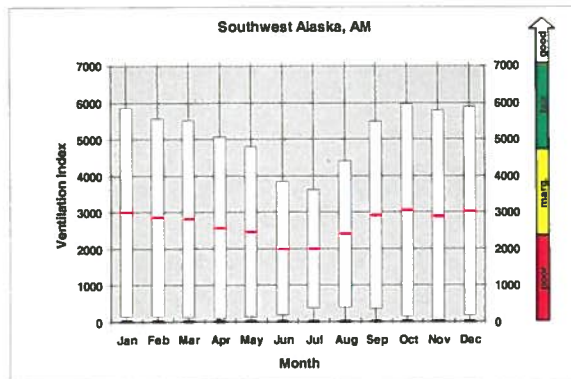
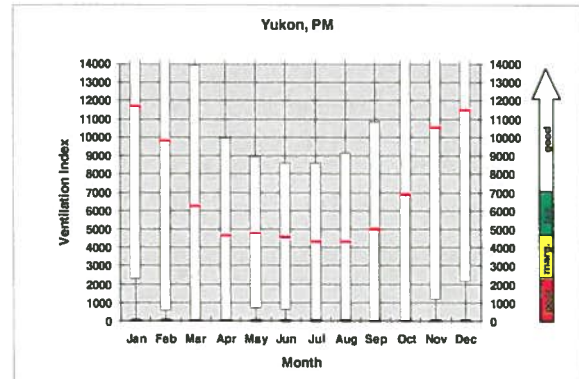
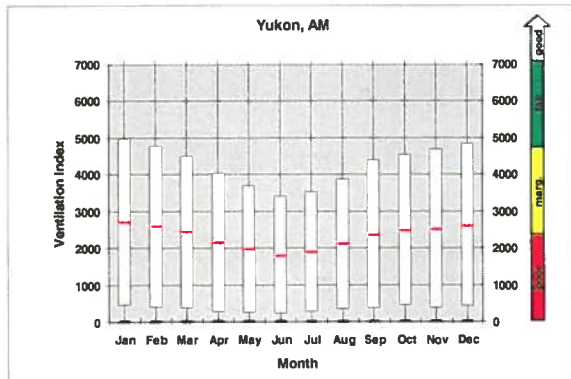
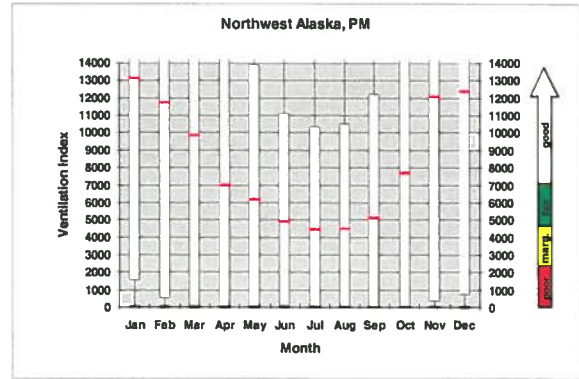
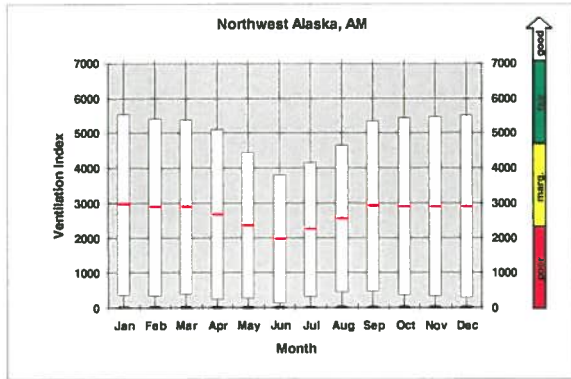
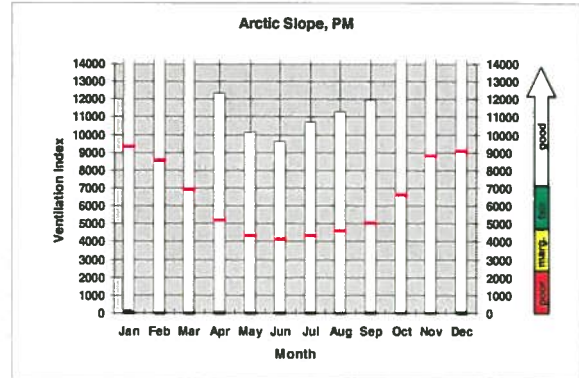
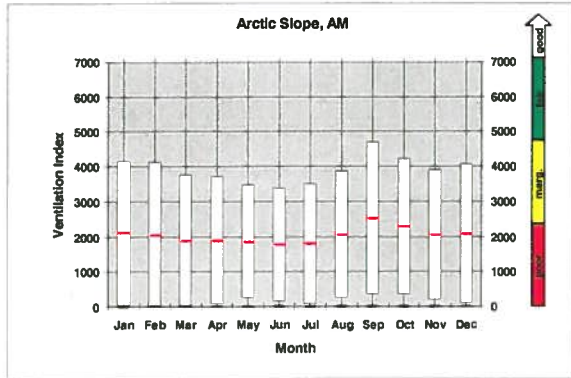


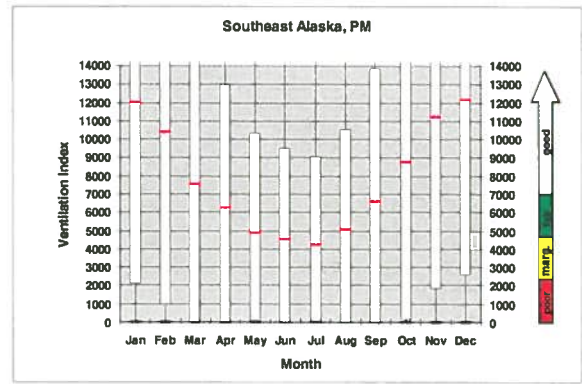
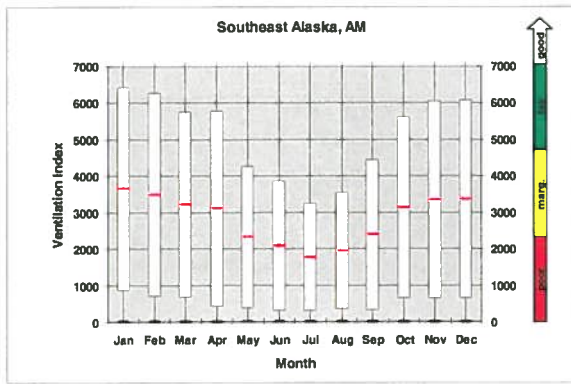
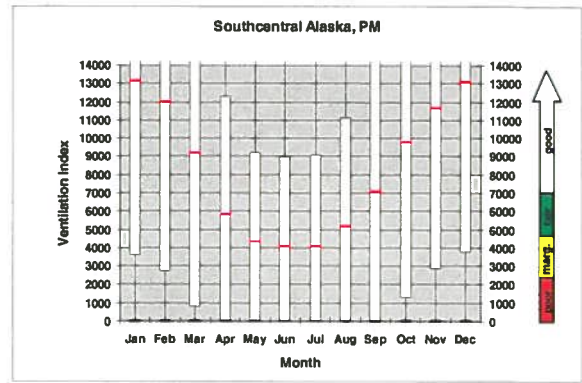
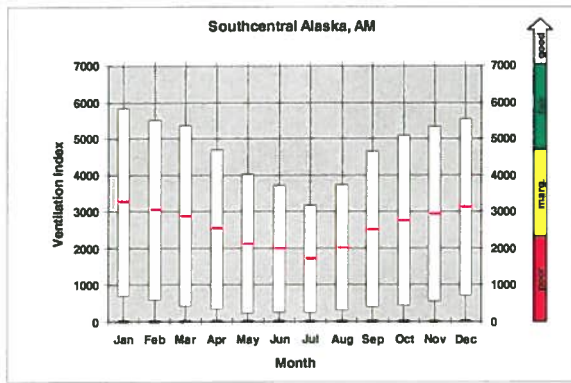




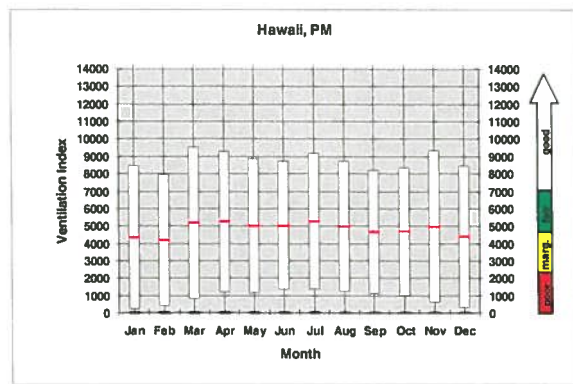
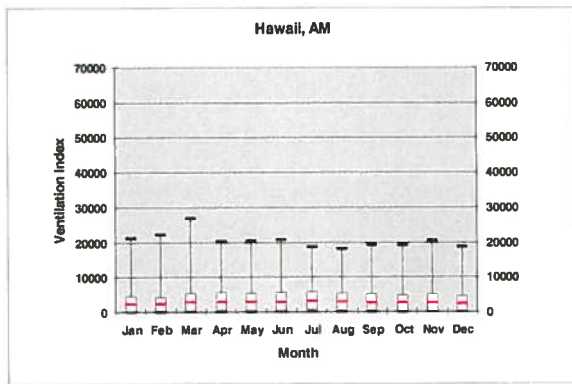


### A3.2 Alaska





### A3.3 Hawaii



## APPENDIX 4: The VCIS Internet Map Server

<http://www.fs.fed.us/pnw/fera/vent>

The home page [www.fs.fed.us/pnw/fera/vent](http://www.fs.fed.us/pnw/fera/vent) provides access to all documentation, maps, and graphs on the ventilation climate information system (VCIS) and the associated assessment of values air quality and visibility at risk from wildland fire.

The “Maps and Graphs” button allows access to summary statistics of over 100 GigaBytes of data through ArcIMS, the ArcInfo Internet Mapping Service by ESRI.

- Alaska, Hawaii, and the 48-states are separate sites because their maps are projected differently.
- A current browser is needed for the Maps and Graphs section (Version 5 or greater of Explorer or Version 6 or greater of Netscape).
- The ArcIMS Maps and Graphs window is separate from other pages at this site. Therefore, the back button on your browser will not work.
- On selecting Alaska, Hawaii, or the 48-states, enlarge the browser window before the site map is loaded. You will be disappointed if you try to enlarge the window after the main map has loaded because the map will remain the original size and not fill the frame.
- ArcIMS is relatively slow. Therefore, the site works best with a direction connection to the Internet rather than through a telephone.
- Use the buttons at the top of the Maps and Graphs window to navigate through the map frame.



Toggle on or off the inset map.



Zoom in. After selecting this button, you can either 1) click a point on the map to center an interval zoom or 2) define the zoom area by clicking on one corner and holding the left mouse button while dragging open a box. Zooming closer and adding map features allows exact points to be selected. Close zooms also help illustrate the resolution of the data.



Zoom out.



Zoom to full extent.



Go back to last extent.



Pan. Move the map across the screen



**Print.** This requires a few moments as it creates a new frame from which you can print just the map and scale or save it to a file.

**GET  
STATS**

Opens a table of buttons to retrieve statistics on all meteorological variables and all times for a selected point on the map.

- There are over 100 GigaBytes of data that the system processes. Therefore, retrieving statistics may require a few moments, especially if connected via telephone.
  - Click on a button for a time and variable of interest to view a plot of the historical frequency.
  - Click on an open graph to reduce its size.
  - You can print or save all open graphs by selecting the Print button at the top of the table.
- Use the Legend on the right to build a map of interest.
    - Select the meteorological base map, monthly mean surface wind, mixing height, or ventilation index.
      - Select the time and month of interest.
      - Check box next to the meteorological window.
      - Click the “Refresh Map” button.
    - Check box next to features to add then click “Refresh Map” button.
  - It may be possible to import a map that was built from VCIS into an ArcInfo application. This feature currently is untested.
  - To save a map or graph, right click over the image and select “Save Picture As” or “Save Image As.” For maps this works best from the print window. You can save graphs from any window.